Project funded by the European Commission under the 6th (EC) RTD Framework Programme (2002- 2006) within the framework of the specific research and technological development programme “Integrating and strengthening the European Research Area”

Project UpWind

Contract No.:
019945 (SES6)

“Integrated Wind Turbine Design”

RESEARCH REPORT on MODELS for NUMERICAL EVALUATION of VARIABLE SPEED DIFFERENT WIND GENERATOR SYSTEMS

(Deliverable No.: D 1B2.b.2)

AUTHOR:	H. Li[1], Z. Chen[1], Henk Polinder[2]
AFFILIATION:	Aalborg University[1], Delft University of Technology[2]
ADDRESS:	Aalborg East DK-9220, Denmark[1], 2628CD Delft, the Netherlands[2]
TEL.:	+45 96359255[1]
EMAIL:	lih@iet.aau.dk, zch@iet.aau.dk, H.Polinder@ewi.tudelft.nl
FURTHER AUTHORS:	
REVIEWER:	Project members
APPROVER:	

Document Information

DOCUMENT TYPE	Help desk document
DOCUMENT NAME:	
REVISION:	
REV.DATE:	
CLASSIFICATION:	R1: Restricted to project members
STATUS:	

Abstract:

Wind energy is currently one of the most cost-effective energy sources to produce electricity among various renewable energy sources. During last two decades, various wind turbine concepts with different generator systems have been developed and built. It is necessary to identify the most cost-effective wind conversion system among the various possible configurations. The aim of this project is to evaluate the suitable cost- effective wind generator systems by using the optimization designs and the numerical comparison. The research report is made of two parts, one focus on the design models of different wind generator systems, the other presents the optimization results and evaluation of variable speed wind generator systems. In this report, firstly, it gives an overview of various wind generator topologies, including their advantages and disadvantages, market status and developing trends. Next, the analytical models include the wind turbine power characteristics; the single/three-stage gearbox and the power electronic converter for possible wind turbine concepts are described. Finally, the electromagnetic design models of the investigated generator topologies are presented, including the squirrel cage induction generator (SCIG), the doubly-fed induction generator (DFIG), the electrically excited synchronous generator (EESG) and permanent magnet synchronous generator (PMSG). Numerical evaluation with optimized design and comparison of variable speed wind generator systems by using the presented models will be introduced in report 2.

Contents

STATUS, CONFIDENTIALITY AND ACCESSIBILITY											
Status				**Confidentiality**				**Accessibility**			
S0	Approved/Released			**R0**	General public			Private web site			
S1	Reviewed			**R1**	Restricted to project members			Public web site			
S2	Pending for review			**R2**	Restricted to European. Commission			Paper copy			
S3	Draft for commends			**R3**	Restricted to WP members + PL						
S4	Under preparation			**R4**	Restricted to Task members +WPL+PL						

PL: *Project leader* **WPL:** *Work package leader* **TL:** *Task leader*

1. Introduction

Wind energy is the world's fastest growing renewable energy source. The average annual growth rate of wind turbine installation is around 30% during last ten years [1] [2]. At the end of 2006, the global wind electricity-generating capacity increased to 74,223 megawatts (MW) from 59,091MW in 2005 (See Fig.1-1). By the end of 2020, it is expected that this figure will increase to well over 1,260,000MW, which will be sufficient for 12% of the world's electricity consumption [3] [4]. Fig. 1-2 depicts the total wind power installed capacity for some countries from the year of 1985 to 2006. The countries with the highest total installed capacity are Germany (20,622 MW), Spain (11,615 MW), USA (11,603 MW), India (6,270 MW) and Denmark (3,136 MW). According to Global Wind Energy Council (GWEC) report [2], Europe continues to lead the market with 48,545 MW of installed capacity at the end of 2006, representing 65 % of the global total installation. The European Wind Energy Association (EWEA) has set a target of satisfying 23% European electricity needs with wind energy by 2030. It is clear that the global market for the electrical power produced by wind turbines has been increasing steadily, which directly pushes the wind generation technology into a more competitive area.

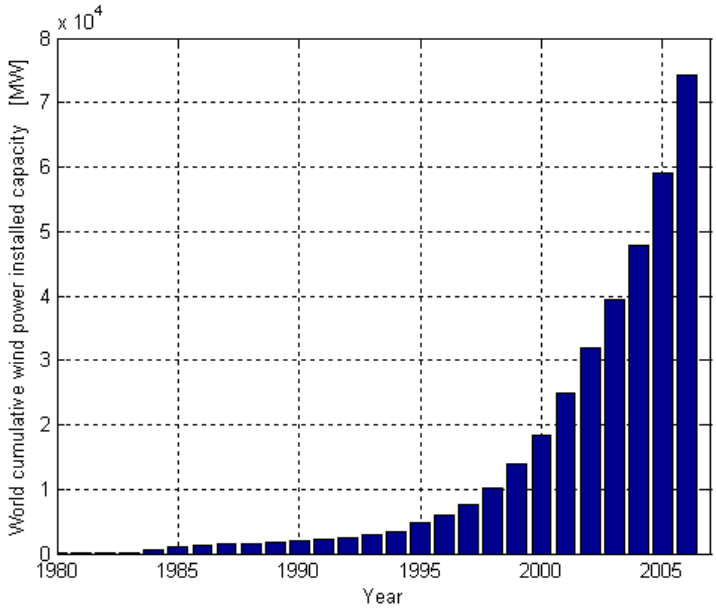

Fig. 1-1: *World cumulative wind power installed capacity (1980-2006)*

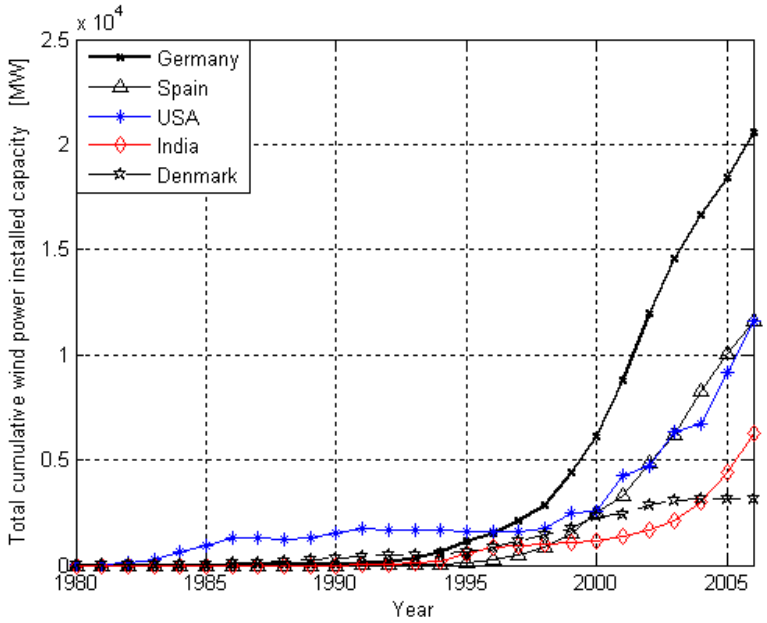

Fig. 1-2: *Total cumulative wind power installed capacity for different countries (1980-2006)*

With rapid development of wind power technologies and significant growth of wind power capacity installed worldwide, various wind turbine concepts have been developed and different wind generators have been built during last two decades. Three types of typical generator systems for large wind turbines exist [3, 5-7]. The first type is a fixed-speed wind turbine system using a multi-stage gearbox and a standard squirrel-cage induction generator (SCIG), directly connected to the grid. The second type is a variable speed wind turbine system with a multi-stage gearbox and a doubly fed induction generator (DFIG), where the power electronic converter feeding the rotor winding has a power rating of approximate 30% of the generator capacity, and the stator winding of the DFIG is directly connected to the grid. The third type is also a variable speed wind turbine, but it is a gearless wind turbine system, normally a low-speed high-torque synchronous generator and a full-scale power electronic converter are used. Additionally, a variety of innovative concepts of wind turbines appear, for example, an interesting alternative may be a mixed solution with a gearbox and a medium low speed PM synchronous generator (PMSG) [7-9], because direct-drive wind generators are becoming larger and even more expensive for increasing power levels and decreasing rotor speeds.

The wind energy conversion system is demanded to be more cost-competitive with other traditional sources of electrical energy, such as coal, gas and nuclear generations, so that comparison of different wind generator configurations are necessary. In order to make a numerical evaluation for different wind generator systems, this report presents the analytical models of various wind generator systems. Based on the presented analytical models in this report, the design optimization and comparison of different wind generator systems will be introduced in report 2.

This report is organized as follows.

Section 2 provides an overall perspective on various types of possible generator configurations and existing wind generator systems. The market status and trends of various types of wind generators are presented.

Section 3 presents drive-train models of wind turbines and power electronic converter models, including the wind turbine characteristics, single-stage or three-stage gearbox models.

Section 4 gives the electromagnetic design models of introduction generators, including SCIG and DFIG.

Section 5 gives the electromagnetic design models of synchronous generators, including EESG and PMSG.

Section 6 presents the summarization and conclusions of this report

2. Overview of different generator types for wind turbines

The goal of this section is to present an overall perspective on various types of possible generator configurations and existing wind generator systems. The market status and trends of various types of wind generators are also analyzed. The section 2 outline is as follows:

2.1 Induction generator concepts: This subsection introduces the basic configurations, advantages and disadvantages of SCIG and DFIG.

2.2 Synchronous generator concepts: This subsection introduces the basic configurations, advantages and disadvantages of EESG and PMSG. The possible configurations and comparisons of PMSG are also investigated.

2.3 Other potential generator concepts: This subsection briefly introduces some possible types of wind turbine generators, such as linear induction generators, switched reluctance generators, brushless doubly fed induction generators, and so on.

2.4 Wind generator systems trends: This subsection gives the market status and trends of various types of generators for wind turbine applications, and presents wind generator configurations to be investigated in this project.

2.1 Induction generator concepts

2.1.1 SCIG topologies

For a long time, squirrel cage induction generators (SCIGs) have been the mostly used generator types for wind turbines. The generator is directly grid connected, which was the conventional concept applied by many Danish wind turbine manufacturers during the 1980's and 1990's, i.e. an upwind, stall regulated, three bladed wind turbine concept using a SCIG, it is sometimes referred to as the "Danish concept" [10]. Since the SCIG always draws reactive power from the grid, during the 1980's this concept was extended with a capacitor bank for reactive power compensation. Smoother grid connection was also achieved by incorporating a soft-starter. Because the generator operation is only stable in the narrow range around the synchronous speed, the wind turbine equipped with this type of generator is often called fixed-speed system. The induced rotor current causes dissipation of electrical energy in the rotor bars. In general, the pole pair number is mostly equal to 2 or 3 in this type commercial fixed-speed wind turbine with SCIG, so that the synchronous speed in a 50Hz-grid is equal to 1500 or 1000 rpm. Therefore, a three-stage gearbox in the drive train is usually required. Furthermore, a pole changeable SCIG has been used, which leads two rotation speeds. The grid connection scheme of a fixed speed wind turbine with SCIG is shown in Fig. 2-1. Some manufacturers, such as Micon (currently merged into Vestas), Bonus (currently Siemens), Made, and Nordex, have products based on this concept.

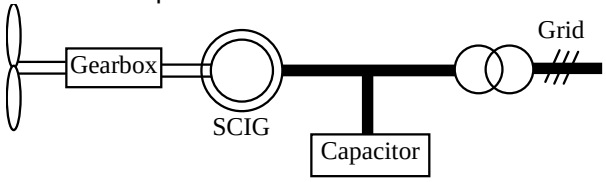

Fig. 2-1: *Scheme of a fixed speed wind concept with SCIG system*

The disadvantages of SCIG for "Danish concept" wind turbines are as follows [10-15]:

• The speed is not controllable and variable only over a very narrow range, in which only speeds higher than the synchronous speed are possible for generator operation. Because a higher slip means a higher dissipation of electrical energy in the rotor bars, for example, the slip is normally not higher than 1% for 1 MW wind turbine [11]. Additionally the fixed speed concept

means that wind speed fluctuations are directly translated into electromechanical torque variations, this causes high mechanical and fatigue stresses on the system (turbine blades, gearbox and generator), and may result in swing oscillations between turbine and generator shaft. Also the periodical torque dips due to the tower shadow and shear effect are not damped by speed variations, and result in higher flicker. Fluctuations in power output are hardly damped. On the other hand, the turbine speed cannot be adjusted to the wind speed to optimize the aerodynamic efficiency. Though a pole changeable SCIG has been applied for this wind turbine concept, it can not still provide continuous speed variations.

• In general, a three-stage gearbox in the drive train is necessary. Gearboxes represent a large mass in the nacelle, and also a large fraction of the investment costs. They are relatively maintenance intensive and a possible source of failure.

• It is necessary to obtain the excitation current from the stator terminal. This makes it impossible to support grid voltage control. In most cases, capacitors are connected in parallel to the generator to compensate for the reactive power consumption.

In addition, in order to fulfil variable speed operation with a SCIG, the capacitor bank and soft-starter are replaced by a full-scale frequency converter, which enables variable speed operation at all wind speeds and does not need to keep its output frequency as the same as the grid frequency. This configuration is the other type of wind turbines with a traditional SCIG. However, compared with the “Danish concept”, its drawback is the high cost of the full-rated converter. In this project, the variable speed wind turbine concept with SCIG is also investigated to compare with other concepts.

2.1.2 DFIG topologies

The doubly fed induction generator (DFIG) is one of the most popular generator types for large wind turbines, since the rating of the converter could be reduced to roughly 30%. The grid-connection scheme of a variable speed wind turbine with DFIG is shown in Fig. 2-2.

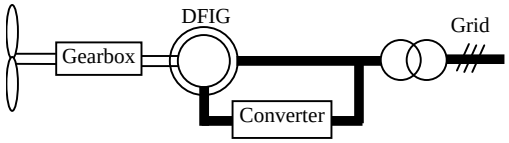

Fig. 2-2: *Scheme of a DFIG system with a three-stage gearbox*

The stator is constructed in the same way as in the SCIG. The rotor is no longer a squirrel cage rotor, but equipped with a three-phase winding (so-called the wound rotor induction generator: WRIG), connected to the grid through a power electronic converter. Typically, by controlling the rotor active power flow direction, the variable speed range $\pm$ 30% around the synchronous speed can be controlled. Instead of dissipating the rotor energy, it can be fed into the grid. The choice for the rated power of the rotor converter is a trade-off between the cost and the desired speed range. The cost of power electronic converters increases fast with increasing rating. Mostly its rating is around 30% of the total generator rated power [13]. Moreover, this converter performs reactive power compensation and smooth grid connection.

The advantages of a DFIG are that the speed is variable within a sufficient range with limited converter costs. The stator active and reactive power can be controlled independently by controlling the rotor currents with the converter. Furthermore, the grid-side converter can control its reactive power to the grid independently of the generator operation. This allows the performance of voltage support towards the grid.

The drawbacks of a DFIG are as follows [10-15]:

• A multi-stage gearbox is still necessary in the drive train, because the speed range of a DFIG without a gearbox is far away from a common turbine speed of 10-25 rpm.

• The control of the rotor power by means of a grid-connected converter requires an electrical connection between a rotating system and a stationary system, such a connection is given by carbon brushes (on the stationary system) pressing against slip rings (rotating system). These require regular maintenance, are a potential cause of machine failure and increase the electrical losses.

• The power electronic converter is also a fragile component because it is very sensitive to over currents. In case of a grid voltage dip, the stator and rotor currents may dramatically increase for a short time (~100 ms). The high machine currents during the protective operations may cause high torque loads on the drive train. The insulated winding on the rotor may be subjected to a stress arising from the rotation and vibration, which may reduce the lifetime of the generator.

• In case of grid disturbances, the ride-through capability of DFIG is required so that the control strategies may be very complex. Detailed transient models and good knowledge of the DFIG parameters are required to make a correct estimate of occurring torques and speed [15].

As it may be mentioned, a precursor of the DFIG is the OptiSlip generator, developed by Vestas since the mid 1990's [10-12]. The basic idea of this concept is to control the rotor resistance using a variable external rotor resistance by means of a power electronic converter. It is basically a single-fed induction generator with the same characteristics as a SCIG. With the power electronic converter mounted on the rotor shaft, it is possible to control the slip (by controlling the external rotor resistance) over a 10% range [12]. The most suitable torque-speed characteristic can be chosen to obtain the optimal speed at the operating point. Only speeds higher than synchronous speed are possible for generator operation, and the rotor power is not fed back into the grid.

2.2 Synchronous generator concepts

Synchronous generators are also candidates in wind generation systems [16-18]. Like the SCIG and DFIG, the synchronous generator generally has a stator magnetic circuit made of laminations provided with uniform slots that house a three-phase winding. For the rotor, there are two main possibilities to choose. One type is a rotor winding supplied by a DC current from a separate circuit, usually called the electrically excited synchronous generator (EESG); and the other type is permanent magnets (PMs) attached to the rotor.

2.2.1 EESG topologies

The EESG is usually built with a rotor carrying a DC field excitation system. The stator carries a three-phase winding quite similar to that of an induction machine. The rotor may have salient poles, or may be cylindrical. Salient poles are more usual in low speed machines, and may be the most useful version for application to wind turbine generators. The grid connection scheme of an EESG for direct-drive wind turbine is shown in Fig. 2-3.

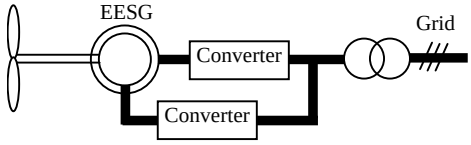

Fig. 2-3: *Scheme of a direct-drive EESG system*

All power generated is processed through a power electronic converter, the interface between generator and grid. At the generator side of the converter, amplitude and frequency of the voltage can be fully controlled by the converter, independently of the grid characteristics. The generator speed is fully controllable over a wide range, even to very low speeds. The gearbox

may thus be omitted. The generator is directly driven by the turbine, hence named as ‘direct drive’. This is an advantage because the gearbox normally has a non-negligible manufacturing cost, generates some acoustic noise, requires regular maintenance (lubrication) and is also a potential cause of mechanical failure. In addition, the other advantage is that the converter permits very flexible control of the entire system. The generator speed, active and reactive power can be fully controlled in case of normal and disturbed grid conditions.

The main drawback of this option is the system cost, both generator and power electronic converter are considerable more expensive than a DFIG system. The converter has to process all the generator power which requires more expensive power electronic components and needs intensive cooling. Furthermore, the generator needs a specific design and high cost: compared with normal electrical machines, it has to supply high electrical torques at low speeds. The diameter of the EESG in large wind turbines will be large. Direct-drive EESG typically has a large rotor diameter (nearly 12 m for the Enercon E-112 direct drive 4.5 MW turbine [18]). The pole pitch must be large enough for this specific design in order to arrange space for the excitation windings and pole shoes. So the larger number of parts and windings probably make it an expensive solution. In addition, it is necessary to excite the rotor winding with DC, using slip rings and brushes, or brushless exciter, employing a rotating rectifier [15].

2.2.2 PMSG topologies

Compared with electrically excited machines, PM machines have a number of economical and technical advantages, so that they are becoming more attractive for direct-drive wind turbines. The advantages over electrically excited machines can be summarized as follows [16-23]:

- Higher efficiency and energy yield.
- No additional power supply for the magnet field excitation.
- Improvement in the efficiency and thermal characteristics of the machines due to absence of the field losses.
- Higher reliability due to the absence of slip rings.
- Higher torque density and improvement in the dynamics of the drive due to the replacement of wound iron mover with high-energy permanent magnet, comparing with the EESG

Though the PMSG can offer a high potential increase in torque density, and is thus a promising technology for future wind turbines, the commercial applications for large turbines are nowadays very limited. The following barriers for commercial development of this type of generator could be identified [16-20]:

- Relatively new and unknown technology for applications in larger MW-range
- Difficult assembly of the generator and high material costs of the magnets
- Low material reliability in harsh atmospheric conditions (offshore)
- Demagnetization of PM at high temperature

In recent years, the use of PM materials is more attractive than before, because the performance of PM materials is improving and the cost of PM materials is decreasing. The trends make PM machines with a full-scale power converter more attractive for direct-drive wind turbines. The grid connection scheme of the direct-drive wind turbine with PMSG is shown in Fig. 2-4. Currently, Zephyros (currently Harakosan) and Mitsubishi are using this concept in 2 MW wind turbines on the market.

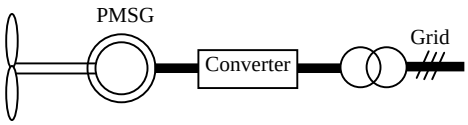

Fig. 2-4: *Scheme of a direct-drive PMSG system*

PM machines are not standard off-the-shelf machines, and allow a great deal of flexibility in their geometry, so that various different topologies may be used. Types of PM machines can be classified into the radial-flux, the axial-flux and the transversal-flux PM machines by the direction of flux penetration. Some basic structures and features from literatures [16-28] are briefly described and summarized as follows.

1. Radial-flux PM (RFPM) machines

The permanent magnets of radial-flux machines are radically oriented. When using radial-flux permanent magnet (RFPM) machines for direct-drive wind turbines, the wind generator system can operate with a good performance over a wide range of speeds. In manufacture, the simple way of constructing the machine with high number of poles is gluing permanent magnets on the rotor surface. In RFPM machines, the length of the machine and the air-gap diameter can be chosen independently. If necessary, the radial-flux machine can be made with a small diameter by using a long machine. RFPM machines have advantages as a better torque density than the EESG, so that some types of RFPM machines have been discussed in a number of literatures.

Two types of RFPM machines, the slotted surface mounted PM machine and the slotted flux concentrating PM machine, have been mostly discussed in references [16] [23]. The rotor design with surface-mounted magnets and the rotor design with flux concentration are shown in Fig. 2-5 Compared with the flux concentration; magnets on the rotor surface have to have a remanent flux density higher than the required air gap flux density, this lead to a very simple rotor design with a lower weight.

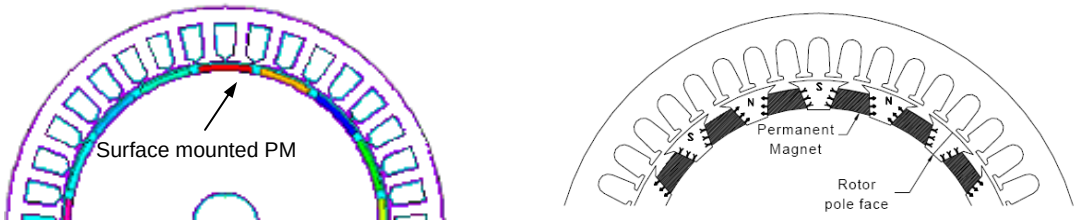

a) *b)*

Fig. 2-5: *Basic configurations of RFPM machines with surface mounted (a) and flux concentrating (b)*

References [16], [17], [20]and [27] discussed RFPM machines with surface mounted magnet, which seems to be a good choice for the design of large scale direct-drive wind turbines. RFPM machines with flux concentration have been discussed and compared with surface mounted RFPM machines in [26] [29]. In addition, Chen et al [20] have presented an outer rotor design for this type of generator in stand alone applications. Several advantages of the outer-rotor RFPM machine were identified in this reference, for example, compared with the inner-rotor construction, the multi-pole structure can be easily accommodated due to the enlarged periphery of the outer-rotor drum, and therefore the total length of the magnetic path can be reduced. As the rotor is directly exposed to the wind, the cooling condition can be improved for the magnets so that the resistance to temperature demagnetization is enhanced. Moreover, Chen et al. [19] have also made a comparison of different PM wind generator topologies. In addition, Hanitsch and Korouji [21] have designed a rare-earth RFPM wind-energy generator with a new topology, which is constructed from two rotors and one stator with short end windings. It can improve the performance of the machine by reducing the weight, increasing the efficiency and reducing the cost of active materials.

2. Axial-flux PM (AFPM) machines

The axial-flux permanent magnet (AFPM) machine is a machine producing magnetic flux in the axial direction, instead of the radial direction. Two types of AFPM machines, the slotless and slotted surface mounted PM, have been mostly discussed in references. Compared with RFPM machines, the advantages of AFPM machines can be summarized as follows:

- Simple winding
- Low cogging torque and noise (in slotless machine)
- Short axial length
- Higher torque/volume ratio

However, the disadvantages of AFPM machines in comparison with RFPM machines are as follows [23] [26] [27]:

- Lower torque/mass ratio
- Larger outer diameter, large amount of PM, and structural instability (in slotless machine)
- Difficulty to maintain air-gap in large diameter (in slotted machine)
- Difficult production of stator core (in slotted machine)

The possibility and potential of AFPM machines for large scale direct-drive wind turbines have been discussed, and some different structures of AFPM machines with surface mounted PM have also been presented in some references [19] [22] [26]

The slotless single-stator double-rotor is a typical structure of slotless AFPM machines [22] [30], which is often referred to as a Torus machine, as shown in Fig. 2-6. The two rotor discs are made of mild steel and have surface-mounted PM to produce an axially directed magnetic field in the machine air gaps. The machine stator comprises a slotless toroidally wound strip-iron core that carries a three-phase winding in a toroidal fashion by means of concentrated coils. The slotless, toroidal-stator, AFPM generator has been also discussed with several advantages, such as the lightness, the compactness, the short axial length, the suitable integration with the engine and others by Spooner and Wu et al. [30-32], the machine's short axial length tends to give it a high power to weight ratio. Parviainen [26] has presented an analytical method to perform the preliminary design of a surface mounted, low speed, slotted AFPM machine with one-rotor-two-stators configuration, as shown in Fig. 2-7. The performance and construction between the low speed radial flux and axial flux PM machine were also compared in the power range from 10 kW to 500kW at 150-600 rpm [26].

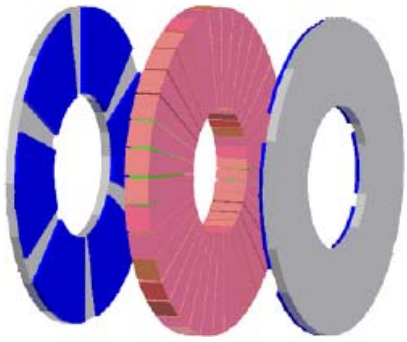

Fig. 2-6: *A slotless single-stator double-rotor AFPM configuration [22]*

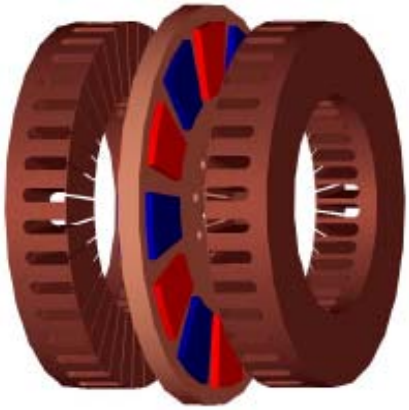

Fig. 2-7: *A slotted double-stator single-rotor AFPM configuration [26]*

Moreover, five different topologies of AFPM machines, a double-stator slotted type, a double-rotor slotted type, a single-sided AFPM with stator balance, a single-sided AFPM with rotor balance, and a slotless single-stator double-rotor (Torus machine), have been investigated and compared with RFPM machines by Chen et al. [19]. According to [19], the two-sided AFPM machine is superior to the one-sided AFPM machine; however, one-sided constructions use less copper and have a lower conduction loss. The Torus construction is simple; however, it requires more magnet weight because of the presence of the additional air gap for accommodating stator windings. As the power rating increases, both the air gap and air gap reluctance become larger, so that this construction is more suitable for low power rating wind generators. In addition, the potential application of soft magnetic composite (SMC) material applied to the low speed, direct-drive axial flux PM wind generator was also discussed by Chen et al. Comparative design studies were conducted on different configuration PM generators with both lamination core and SMC core [33].

3. Transversal-flux PM (TFPM) machines

The transverse-flux principle means that the path of the magnetic flux is perpendicular to the direction of the rotor rotation. There are also some different rotor structures for this technology, such as the rotor with single-sided surface magnets, with single-sided flux concentration and with double-sided flux concentration. Fig. 2-8 shows the configuration of a surface-mounted transverse-flux PM machine (TFPM) [12]. A TFPM machine is a synchronous machine in nature, and it will function in a similar manner to any other PMSG in principle. Compared with longitudinal machines, TFPM machines have some advantages, such as higher torque density, considerably low copper losses and simple winding. However, the torque density of TFPM machines with large air-gap may be a little high or even low depending on the outsider diameter [16] [23]. The construction of TFPM machines is much more complicated.

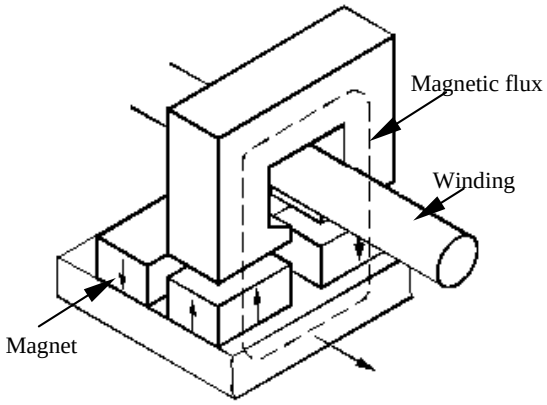

Fig. 2-8: *Surface-mounted transverse-flux PM structure [16]*

Compared with RFPM or AFPM machines, a major difference is that TFPM machines allow an increase in the space for the simple windings without decreasing the available space for the main flux, and so that the machines have very low copper losses. TFPM machines can also be made with a very small pole pitch, however, the electromagnetic structure is much more complicated. TFPM machines have also the low power factor, which leads to an increase in the necessary rating of the power electronic converter.

TFPM machines have been discussed in a number of references [16] [23] [27] [34] [35]. References [16] [27] show that the weight of a 55 kW TFPM machine is about half of the total weight of an asynchronous machine with a gearbox. TFPM machines seem to be suitable for direct-drive applications because of the high specific torque, although special methods of manufacturing and assembly are required [23]. Harris et al. [34] compared the advantages and disadvantages of three different TFPM machine topologies, which include a single sided surface mounted PM machine, a single sided surface mounted PM machine with stator bridges, and a double sided flux concentrating PM machine.

2.2.3 Other potential generator types

Many other types of wind generators are also mentioned in literatures, such as linear induction generators [36], switched reluctance generators [37], claw pole generators [36]; brushless doubly fed induction generators (BDFIG) [36] [38]. Amongst them, the BDFIG may be one of the most innovative types. For this configuration, the output of the induction generator is directly connected to the grid, and thus the generator output frequency must be equal to the grid frequency. The BDFIG does not need the slip-ring; however, it requires double stator windings with different number of poles, respectively. The second stator layer has generally lower copper mass, because only a part of the generator nominal current flows in the second winding. This second stator winding is connected through a power electronic converter, which is rated at only a fraction of the wind turbine rating. In addition, the BDFIG system has the capability of realizing the variable speed operation and independently controls the stator active and reactive power. Compared with the DFIG system, this concept does not require slip-rings, however, the machine operation principle and its assembly are relatively complex.

2.3 Wind generator systems trends

2.3.1 Market penetration of different wind turbine concepts

Various types of wind turbines have been on the market with different power levels. In order to present the trends of different wind generator systems on the market, Table 2-1 shows some wind turbines with a rated power over 2 MW from different manufactures, such as Vestas, Gamesa, GE wind, Repower, Nordex and so on, where the wind turbine concept, generator type, rated power and turbine rotor speed are obtained from manufacturers' websites [39-51].

Table 2-1: *Large wind turbine concepts on the market over 2 MW*

Wind turbine concept	Generator Type	Power/Rotor diameter/Speed	Manufacturer
Variable speed multiple-stage concept with partial-scale power converter	DFIG	4.5 MW /120 m/14.9 rpm	Vestas
		2 MW/90 m/19 rpm	Gamesa
		3.6 MW/104 m/15.3 rpm	GE Wind
		5 MW/126 m/12.1 rpm	Repower

		2.5 MW/90 m/14.85 rpm	Nordex
		3 MW/100 m/14.25 rpm	Ecotecnia
Limited variable speed with multiple-stage gearbox	WRIG	2 MW/88 m/17 rpm	Suzlon
Variable speed multiple-stage gearbox with full-scale power converter	SCIG	3.6 MW/107 m/13 rpm	Siemens Wind Power
	PMSG	2.x MW/88 m/16.5 rpm	GE Wind
Variable speed single-stage gearbox with full-scale power converter	PMSG	5 MW/116 m/14.8 rpm	Multibrid
		3 MW/90 m/16 rpm	Winwind
Variable speed direct-drive with full-scale power converter	EESG	4.5 MW/114 m/13 rpm	Enercon
	PMSG	2 MW/71 m/23 rpm	Zephyros

As it can be seen, most manufactures are using geared-drive wind turbine concepts. The wind turbines produced by Vestas, Gamesa, GE wind, Repower, Nordex, Ecotecnia are using DFIG with a multiple-stage gearbox. According to this survey, it is clear that the wind market is still dominated by DFIG with a multiple-stage gearbox, and the mostly used generator type is still the induction generator (DFIG, SCIG and WRIG). Two companies, Multibrid and WinWind, use PMSG with a single-stage gearbox. Direct-drive wind turbines with EESG and PMSG have been used by Enercon and Zephyros, respectively. According to [3] Vestas maintains its position as the word's largest manufacturer, followed by the Gamesa, Enercon and GE Wind. The world market share at the end of 2004 for each company is 34%, 17%, 15% and 11%.

Fig. 2-9 depicts the market penetration and share of different wind generator systems based on the recorded world suppliers' market data over a 10 year period (1995–2004) [52]. As it can be seen, the fixed speed SCIG system has decreased about threefold over 10 years, from almost 70% in 1995 to almost 25% in 2004. Market penetration of the OptiSlip concept (WRIG in Fig. 4) has declined since 1997 in favour of the more attractive variable speed concept (DFIG). The trend depicted in Fig. 16 clearly indicates that the WRIG type is being phased out of the market. The DFIG wind turbines have increased from 0% to almost 55% of the yearly installed wind power over 10 years, it clearly becomes the most dominant concept at the end of 2004. Market penetration of the SG concept (EESG or PMSG) has altered little over 10 years, with no such dramatic changes as observed for SCIG, WRIG and DFIG. There is, however, a slight increasing trend over the last 3 years (2002–2004). During the 10 years, the direct-drive SG (EESG and PMSG) has ranked third or fourth.

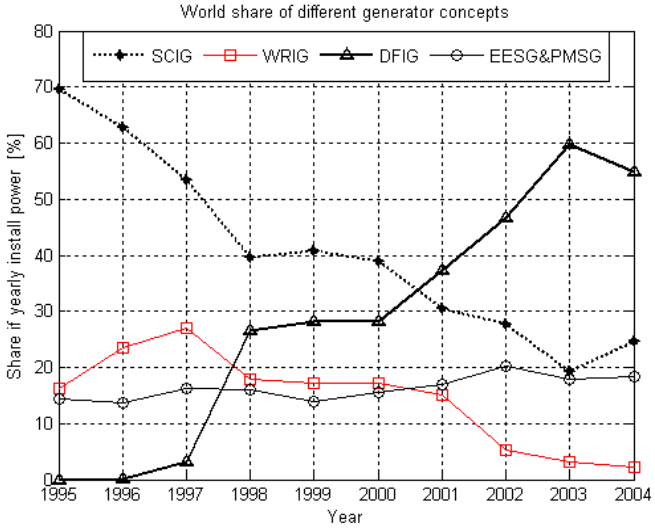

Fig. 2-9: *World share of yearly installed power for different wind generator systems*

2.3.2 Trends discussion

With rapid development of wind turbine technologies, future trends in the wind turbine industry will probably be focused on the gradual improvement of already known technologies, which can be summarized as follows [3] [5] [53] [54] [55]:

- The power level of a single wind turbine will continue to increase, because this reduces the cost of placing wind turbines, especially for offshore wind farms.
- Offshore wind energy is more attractive, due to higher wind speed and more space than on shore wind energy.
- An increasing trend is to remove dispersed single wind turbine in favour of concentrated wind turbines in large wind farms.
- An increasing trend of the penetration of wind power into the power system.

1. Grid connection requirements

The penetration of wind power into the power system continues to increase, which implies the situation of the large wind farms is changing from being simple energy sources to having power plant status with grid support characteristics. One major challenge in the present and coming years is the connection and optimized integration of large wind farms into electrical grids [3]. With increased wind power capacity, Transmission System Operators (TSOs) have become concerned about the impact of high levels of wind power generation in power systems. To handle large-scale integration of wind power, TSOs have issued grid codes and grid requirements for wind turbines connection and operation. The main issues of grid codes can be summarized as follows [10] [11]:

- Active power control.
- Reactive power control.
- Voltage and frequency control.
- Power quality, e.g. flickers and harmonics.
- Fault ride-through capability.

As the above mentioned, the power control capability and the fault ride-through capability are mainly concerned by some TSOs. Wind farms are required to behave as conventional power plants in power systems, such as regulating active and reactive power, and performing frequency and voltage control. Whereas, the fault ride-through capability is required to avoid significant loss of wind power production in the event of grid faults. This means wind turbines should stay connected and contribute to the grid in case of a disturbance such as a voltage dip. They should immediately supply active and reactive power for frequency and voltage recovery after the fault has been cleared. As an example, the requirements concerning immunity to voltage dips as prescribed by E.ON Netz, a grid operator in Northern Germany, is shown in Fig. 2-10. Only when the grid voltage drops below the curve (in duration or voltage level), the turbine is allowed to be disconnected. When the voltage is in the area 1 the turbine should also supply reactive power to the grid in order to support grid restoration [11].

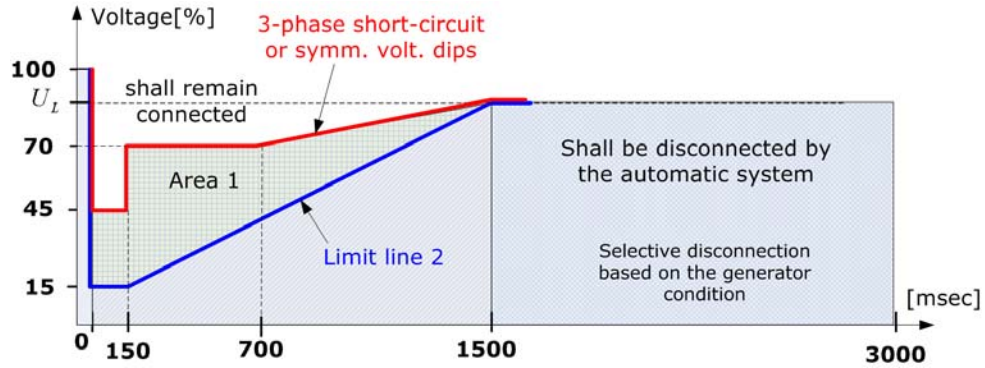

Fig. 2-10: *Voltage dips that wind turbines should be able to handle without disconnection*

2. Trends of wind generator systems

According to the survey of different wind generator systems and considering the grid connection requirements on wind turbines, the developing trends of wind generator systems may be summarized as follows:

- Variable speed concepts

Variable speed operation is very attractive for a number of reasons, including reduced mechanical stress and increased power capture. As mentioned, the market share of the fixed speed concept has decreased slightly while variable speed wind turbine increases. For various variable speed wind turbine concepts, a multiple-stage geared-drive DFIG with a partial-scale power converter is still dominant on the current market. Compared with other variable speed concepts with a full-scale power converter, the main advantage of this concept is only 30% of the generated power passing through the power converter, so that it may have substantial cost advantages even with low-cost power electronics in the future. However, from the viewpoint of the fault ride-through capability, the DFIG system has to endure large peak currents during grid faults, an advanced protection systems may be required. On the contrary, variable speed wind turbines with a full-scale power converter may be more effective and less complicated to deal with grid-related problems. Therefore, variable speed wind turbine concepts with a full-scale power converter will become more attractive.

- Direct-drive concepts

Compared with geared-drive wind generator systems, the main advantages of direct-drive wind generator systems are higher overall efficiency, reliability and availability due to omitting the gearbox. Though the size of direct-drive generator is usually larger, it may not be a serious disadvantage for the offshore wind energy.

- PM excited generator types

PM machines are more attractive and superior with higher efficiency and energy yield, higher reliability and power to weight ratio compared with electrically excited machines. According to the above survey of RFPM, AFPM and TFPM machines, RFPM machines with surface mounted PM may be more suitable for direct-drive PM generator types, due to allowing the simple generator structure, good utilization of the active materials, and also allowing the relatively small diameter in comparison with AFPM and TRPM machines. In the case of AFPM machines, the disadvantages as described in subsection 2.2, which make the machine cost increase and manufacturing difficult, must be solved or improved significantly. Although TFPM machines have some advantages, such as high torque density and simple winding with low copper losses, the torque density of TFPM machines with large air-gap may be a little high or even low depending on the outsider diameter [12]. In my opinion, TFPM still have potential to be used as a direct-drive PM generator with new topology design, since the machines are more flexible for new topologies.

Considering the performance of PM materials is improving and the cost of PM material is decreasing in recent years, in addition that the cost of power electronics is decreasing, variable speed direct-drive PM machines with a full-scale power converter become more attractive for offshore wind powers. On the other hand, variable speed concepts with a full-scale power converter and a single- or multiple-stage gearbox drive train may be interesting solutions not only in respect to the annual energy yield per cost but also in respect to the total weight. For example, the market interest of PMSG system with a multiple-stage gearbox or a single-stage gearbox is increasing.

2.3.3 Generator configurations investigated

The further development of variable speed wind turbine concepts would be focused on the optimized wind generator systems and thus moving towards more cost-effective machines. A numerical comparison of different wind generator systems is required to identify the most cost-effective wind energy conversion system.

In this project, the following designs and comparison of seven variable speed wind generator systems are investigated during the study:

- Squirrel cage induction generator (SCIG) systems

(1) *SCIG_3G*: A three-stage gearbox driving a high-speed SCIG system and the generator's electrical output is interfaced to the utility grid with a power electronic (PE) system.

- Doubly fed induction generator (DFIG) systems

(2) *DFIG_3G*: A three-stage gearbox driving a high-speed wound-rotor induction generator, the rotor power of which is processed and coupled to the utility grid by a PE system with a rating about one-third that of the generator.

(3) *DFIG_1G*: A single-stage gearbox driving a medium-speed, wound-rotor induction generator, the rotor power of which is processed and coupled to the utility grid by a PE system with a rating about one-third that of the generator.

- Electrically Excited synchronous generator (EESG) systems

(4) *EESG_DD*: A wind turbine main shaft directly drives a low-speed, high-torque, EESG system. All of the generator's electrical output is processed and coupled to the utility grid by a full-rated PE system.

- Permanent magnet synchronous generator (PMSG) systems

(5) *PMSG_DD*: A wind turbine main shaft directly drives a low-speed, high-torque, PM excited synchronous generator.

(6) *PMSG_1G*: A single-stage gearbox drives a medium-speed, medium-torque, PM excited synchronous generator.

(7) *PMSG_3G*: A three-stage gearbox drives a high-speed, low-torque, PM excited synchronous generator.

Optimization designs and numerical evaluations of the above wind generator systems will be presented in report 2. In this report, the analytical design models and electromagnetic designs of the corresponding wind generator systems are introduced.

3. Modelling of wind turbine drive trains

The goal of this section is to present the analytical models of the components of wind turbines, including the wind turbine power characteristics, the gearbox and the power electronic converter. The section 3 outline is as follows:

3.1 Wind turbine modeling: This subsection introduces the power characteristics of wind turbines. The calculations of annual energy production (AEP) are also described.

3.2 Gearbox modeling: This subsection presents the single-stage and the three-stage gearbox models, including the weight, cost and losses models.

3.3 Power electronic converter modeling: This subsection presents the full scale power converter and the partial scale power converter models, including the cost and losses models

3.1 Wind turbine modelling

The available shaft power, P_T from a wind turbine can be calculated as a function of the wind speed as

$$P_T = \frac{1}{8}\rho C_p(\lambda,\beta)\pi D^2 v^3 \tag{3-1}$$

where ρ is the air density, D is the wind turbine rotor diameter, v is the wind speed, and $C_p(\lambda,\beta)$ is the power coefficient or aerodynamic efficiency, which is a function of the tip-speed ratio, λ and the pitch angel of turbine blades, β .

Fig.3-1 shows a typical power characteristic of a wind turbine.

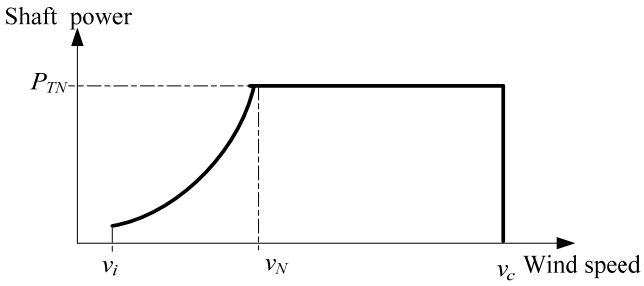

Fig. 3-1: *Power characteristics of a wind turbine*

where v_i is the cut-in wind speed, v_c is the cut-out wind speed. In this case, the shaft power is assumed to be proportional to the cube of the wind speed at the maximum aerodynamic efficiency, $C_{p\max}$ below the rated wind speed. At wind speeds above the rated wind speed, the blades are pitched to reduce the aerodynamic efficiency, and so that the shaft power keeps a constant. The rated wind speed can be calculated as

$$v_N = \sqrt[3]{\frac{8P_{TN}}{\pi\rho C_{p\max} D^2}} \tag{3-2}$$

where P_{TN} is the rated shaft power, which can be calculated by the design optimization of wind generator systems.

For energy yield calculations, the energy contribution at each wind speed can be estimated

by the product of the power output $P_{grid}(v)$ of the wind generator system at a specific wind speed and the duration that the wind speed occurs annually. Therefore, the annual energy production (AEP) can be estimated by summing the incremental energy contributions at each wind speed, which can be expressed as:

$$AEP = 365 \times 24 \cdot \int_{v_i}^{v_c} P_{grid}(v) \cdot f(v)\, dv \quad = 8760 \sum_{j=1}^{n} P_{grid}(v_j)\ f(v_j)\, \Delta v \tag{3-3}$$

where $f(v)$ is Weibull density distribution, which is given as

$$f(v) = \frac{k}{c}\left(\frac{v}{c}\right)^{k-1} e^{(-(v/c)^k)} \qquad (k > 0, c > 1) \tag{3-4}$$

where k is the shape parameter and c is the scale parameter.

The wind speed of candidate sites is usually measured at 10m anemometer height [14]. If these heights do not match the hub height of a wind turbine, it is necessary to extrapolate the wind speeds to the hub height of the turbine. The extrapolated wind speed, v_H corresponding to the hub height is given by [56] [57]

$$v_H = v_0 (H / H_0)^{\alpha} \tag{3-5}$$

where v_0 is the wind speed at height $H_0 = 10$ m above the ground level α is the power index constant. In this case, α is assumed to be 1/7.

The majority of wind farm sites around the world have the annual mean wind speeds in the range of 6-8m/s [7] [57] at 10m height. In this case, the hub height of wind turbine is approximately calculated with 1.2 times of turbine blades diameter. A specific site with an average wind speed of 7m/s at 10m height $(k = 2, c = 7.9)$ is used. The AEP of different wind generator systems can be evaluated by the calculated mean wind speed at the hub height.

3.2 Gearbox modelling

In this subsection, the single-stage planetary gearbox and the three-stage gearbox are described for the wind turbine applications. In the single-stage gearbox, the cost and weight models with the different gear ratios are presented so that the wind generator systems with the optimum gear ratio can be analyzed in this study.

3.2.1 Single-stage gearbox

Fig. 3-2 shows the single-stage gearbox, which consists of a single-stage of double-helical gears, arranged in a planetary configuration [8]. The generator, gearbox, main shaft, and shaft bearing are all integrated within a common housing. The common generator-gearbox housing is supported by a tubular bedplate structure. The single spherical bearing design allows the planet axis to adjust itself to equalize tooth loads even when the carrier is deflected. The sun pinion is fully floating and decoupled from the output by a tubular torque-transmitting member. The tower-top assemblies are enclosed with a non-structural fibreglass nacelle cover [8] [14] [58]. This design achieves very low noise levels without requiring vibration isolation of the gearbox from its bedplate. All of the internal rotating components are pressure-lubricated, including the main shaft bearings and the generator bearings.

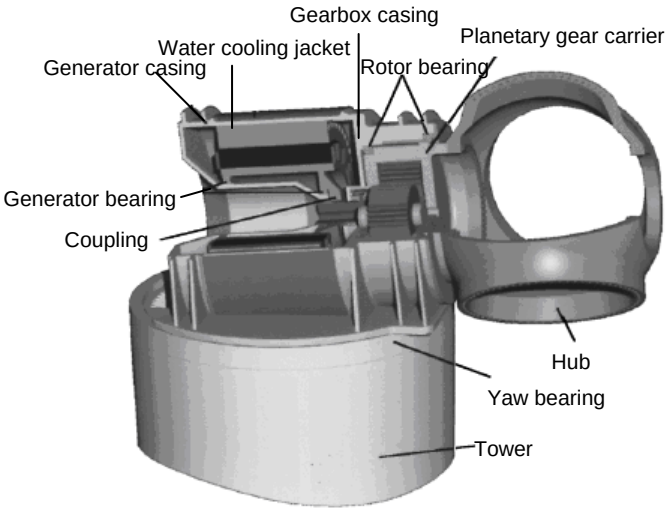

Fig. 3-2: *Configuration of a wind generator design with a single-stage gearbox [8]*

The gears run in an essentially dry-sump mode, reducing churning losses. For start-up and safety, there is a small lubricant pool at the bottom of the ring gears, just enough to dip the planet bearings. The pressurized lubricant is fed through a rotating manifold to the rotating planet carrier, allowing continuous spray lubrication of the planets, the sun tooth meshes, and the planet bearings.

As the gear ratio increases, increasing the generator speed reduces the size and the cost of the generator. However, higher gearbox ratios increase the gearbox mass and cost, so that weight and cost models of the gearbox at different power levels and different gear ratios have to be considered.

The gear trains of the gearbox can be of two distinct types: parallel shaft and planetary. Due to its compact and lightweight, a single-stage planetary configuration (see Fig. 3-2) is used to investigate the most-effective wind generator system with a single-stage gearbox. The weight of a single gearbox stage, G_{gear_1} depends upon the stage ratios chosen and the shaft torque level, which can be given as [7]

$$G_{gear\_1} = 3.2 T_m \, F_s \, F_w \,/ 1000 \tag{3-6}$$

where T_m is the output torque of the single-stage gearbox (Nm); F_s is service factor considerations of surface damage and of failure by metal fatigue. The weight factor, F_w is given as

$$F_w = \frac{1}{Z} + \frac{1}{Z \cdot r_w} + r_w + r_w{}^2 + 0.4 \frac{(1 + r_w)}{Z} (r_{ratio} - 1)^2 \tag{3-7}$$

where Z is the optional number of planet wheels in a stage; the sun wheel ratio $r_w = \frac{r_{ratio}}{2} - 1$, r_{ratio} is the single-stage gear ratio.

The cost of a single-stage gearbox, C_{gear_1} is roughly estimated by its weight and the specific cost, c_{gear_1}

$$C_{gear\_1} = c_{gear\_1} \, G_{gear\_1} \tag{3-8}$$

The losses in a gearbox can be divided into two different parts, one includes gear teeth losses and bearing losses, that depends on the input power, and the other includes seal losses and

lubricant losses, which depends on the rotational speed. For the power dependent losses, they are usually modeled as 1% of the input power, so that it is reasonable to neglect [9]. This means that the main losses in a gearbox are proportional to the shaft speed.

$$p_{gear\_1} = k_{g\_1} P_N \frac{n_r}{n_{rN}} \tag{3-9}$$

where k_{g_1} is a constant for the speed dependent losses of a single-stage gearbox, P_N is the rated power of wind turbines, n_r is the rotor speed, n_{rN} is the rated rotor speed.

The weight and cost models are demonstrated by a 1.5 MW single-stage gearbox, which is presented in report 2.

3.2.2 Three-stage gearbox

Fig. 3-3 depicts the typical configuration of a three-stage gearbox for wind turbine applications [58]. The gearbox consists of one planetary section, the first stage, and two additional stages of parallel-shaft helical gears. The input from the main shaft is fixed to the first-stage carrier with a shrink disc. The gearbox carrier bearings, housed in a member with opposing torque arms, form the support for the main shaft rear. The torque arms are fitted to the bedplate on pins with elastomeric bushings. This mounting helps to attenuate structural borne vibrations, which is useful for meeting stringent noise standards. The sun pinion is spine-connected to the first helical stage. This connection provides a degree of freedom for the inevitable positional displacement of the sun pinion, which is critical for equalizing tooth forces. The connection does, however, cause positional displacement to slope the sun pinion axis. This sensitivity to manufacturing deviations is managed by extreme precision in component machining. Output to the generator is offset, making the main shaft center line clear of the high-speed shaft. This leaves enough room for the slip ring assembly. The gearbox center line must accommodate a conduit of electrical or hydraulic lines, or both, which must be connected to the rotor hub interior.

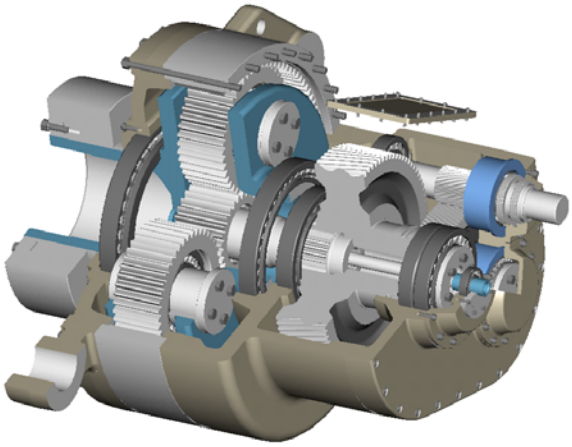

Fig. 3-3: *Configuration of a typical three-stage gearbox for wind turbine applications [58]*

In this case, the mass weight for a three-stage gearbox, G_{gear_3} is scaled based on the low-speed shaft torque, and thus adjusts for differences in rotor diameter and tip speed [59].

$$G_{gear\_3} = 10.35\, T_L + 1950 \tag{3-10}$$

Where T_L is the input mechanical torque of the low speed shaft (kNm). The comparison of the weight calculation of a three-stage gearbox and some weight data from wind turbine products are also given in report 2.

The cost of a three-stage gearbox, C_{gear_3} is also roughly estimated by its weight and the specific cost, c_{gear_3}

$$C_{gear\_3} = c_{gear\_3}\, G_{gear\_3} \tag{3-11}$$

The losses in a thee-stage gearbox are proportional to the shaft speed.

$$p_{gear\_3} = k_{g\_3}\, P_N\, \frac{n_r}{n_{rN}} \tag{3-12}$$

where k_{g_3} is a constant for the speed dependent losses of a three-stage gearbox.

3.3 Power electronic converter modelling

A back-to-back PWM power converter is usually used to make the variable speed operation, and control the active power and the reactive power of wind turbine systems [5]. As an example, Fig.3-4 shows the main circuit topology of a back-to-back PWM power converter of direct-drive PM wind generator system, which is composed of the generator-side converter, the grid-side converter and the dc-link capacitor. By using the power electronic converter, the variable speed operation of wind generator systems can be controlled so that the turbine can operate at its maximum efficiency.

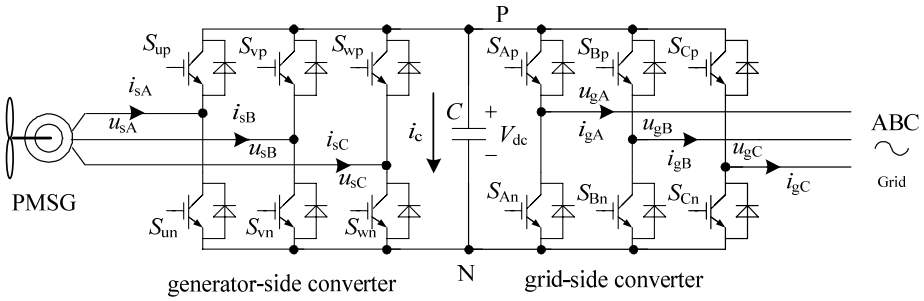

Fig. 3-4: *Main circuit topology of a back-to-back PWM full power converter for PMSG*

The cost of a power electronic converter is a function of power converter rating in kW with a constant k_c (Euro/kW) [9]

$$C_{conv} = k_c\, P_{conv} \tag{3-13}$$

Where P_{conv} is the power converter rating. For the wind generator system with a partial rated power converter, it is assumed to 30% of the wind turbine power rating; for the wind generator system with a full rated power converter, it is assumed to 100% of the wind turbine power rating.

There are various ways of modeling power electronic converter losses [23] [25]. The model used here divides the power losses into three parts [9]:

- A small part that is constant and consists of power dissipated in power supplies, gate drives, control, cooling systems and so on;
- A large part that is proportional to the current and consists of switching losses and conduction losses;
- A part that is proportional to the current squared and consists of conduction losses because the on-state voltage of a semiconductor increases with the current.

In this case, the losses in a power electronic converter, p_{conv} are modeled as [9]

$$p_{conv} = \frac{p_{convN}}{31}(1+10\frac{I_s}{I_{sN}}+5\frac{I_s^2}{I_{sN}^2}+10\frac{I_g}{I_{gN}}+5\frac{I_g^2}{I_{gN}^2}) \quad (3\text{-}14)$$

where p_{convN} is the dissipation in a power electronic converter at the rated power, I_s is the generator side converter current, I_{sN} is the generator side converter rated current, I_g is the grid side converter current, and I_{gN} is the grid side converter rated current.

4. Design models of induction generators

The machine parameters are calculated based on well-known analytical methods using equivalent circuit models. The dimensions of the active parts can be obtained from the conventional magnetic circuit laws. This section is to describe the key analytical models used to determine the induction generator sizes and the important equations used to determine the parameters of the equivalent circuit. More detailed about the calculations are given in [9] [36]. In addition, the corresponding optimization models and the design assumptions will be presented in report 2. This section outline is as follows:

4.1 Model description of SCIG: This subsection introduces the design equations of SCIG, such as the machines basic dimensions, electrical parameters, power losses, mass weights and costs, and so on.

4.2 Model description of DFIG: This subsection introduces the design equations of DFIG, such as the machines basic dimensions, electrical parameters, power losses and mass weights and costs, and so on.

4.1 Model description of SCIG

The slot is described by its height and its width. Fig. 4-1 illustrates the configuration of the stator slot of a SCIG.

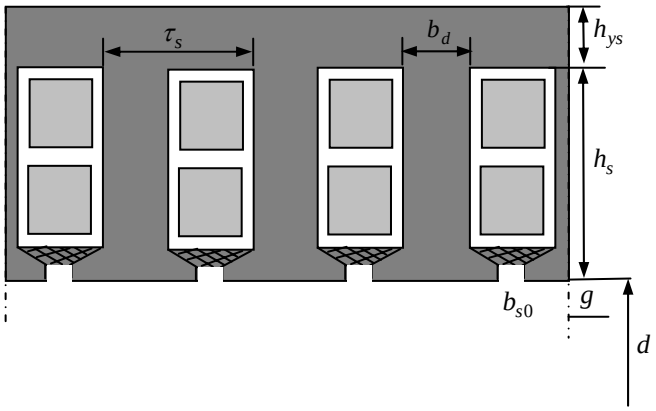

Fig. 4-1: *The stator slot of an induction machine*

1. Basic dimensions

The air gap diameter, d and pole pitch, τ_p determine the number of pole pairs, N_p

$$N_p = \frac{\pi \cdot d}{2 \cdot \tau_p} \tag{4-1}$$

For the machine design, the rated slip of a SCIG, s_N may be set within 1%. A smaller rated slip could result in a lower power loss. For example s_N =-0.002, then the synchronous speed can be determined as

$$n_1 = \frac{n_r}{1 - s_N} = \frac{n_r}{1.002} \tag{4-2}$$

Where n_r is the generator rotor speed (rpm).

The stator slot pitch is

$$\tau_s = \frac{\tau_p}{m \cdot q} \tag{4-3}$$

where m is the phase number of the stator windings; q is the number of slots per pole and phase, in this case q is set to 6 to allow for small additional losses of a SCIG.

The stator yoke thickness, h_{ys} is determined by the allowed flux densities in the stator.

$$h_{ys} = \frac{\hat{B}_{g0} \cdot \tau_p}{\hat{B}_{ys} \cdot \pi} \tag{4-4}$$

Where $\hat{B}_{g0}$ is the peak air gap flux density; $\hat{B}_{ys}$ is the peak stator and rotor yoke flux density. In this case, the rotor yoke thickness is assumed to be the same value of the stator yoke height.

2. Stator resistance and inductance

The phase resistance of the stator winding is calculated as

$$R_s = \frac{\rho_{cu} L_{cus}}{A_{cus}} \tag{4-5}$$

where ρ_{cu} is the resistivity of copper. A_{cus} is the cross-sectional area of the stator conductor, and L_{cus} is the length of the conductor of the stator phase winding, which can be given as

$$L_{cus} = 2 N_s (2 (\tau_p - shortpitch / m / q) + L_t) \tag{4-6}$$

$$A_{cus} = k_{fills} \frac{N_p \; q \, b_s (h_s - h_w)}{N_s} \tag{4-7}$$

Where *shortpitch* is numbers of the stator winding short-pitched; k_{fills} is the stator slot fill factor; L_t is the stator core length; h_w is the slot wedge thickness, N_s is the number of turns of the stator phase winding.

The slot leakage inductance, tooth tip leakage inductance and end winding leakage inductance can be expressed as [36]

$$L_{ssl} = 2 \mu_0 \frac{L_t \; N_s^2}{N_p \; q} \left(\frac{(h_s - 0.003)}{3 b_s} + \frac{0.003}{b_{s0}}\right) \tag{4-8}$$

$$L_{stl} = 2 \mu_0 \frac{L_t \; N_s^2}{N_p \; q} \frac{5 \; g / b_{s0}}{5 + 4 \; g / b_{s0}} \tag{4-9}$$

$$L_{sel} = \mu_0 \frac{1.2 \; N_s^2}{N_p} \left(\frac{2}{3} \tau_p + 0.01\right) \tag{4-10}$$

Where μ_0 is the constant of the permeability of vacuum, b_s is the stator slot width, b_{s0} is the width of the stator slot opening; g the air gap length;

The stator leakage inductance, $L_{s\sigma}$ can be given as the sum of the slot, air-gap, and end-winding leakage inductances.

$$L_{s\sigma} = L_{ssl} + L_{stl} + L_{sel} \tag{4-11}$$

The magnetizing inductance is given as [9] [36]

$$L_{sm} = \frac{6 \cdot \mu_0 \cdot L_t \cdot r_s \cdot (k_w \cdot N_s)^2}{\pi \cdot N_p{}^2 g_{eff}} \tag{4-12}$$

where r_s is the stator radius, k_w is the winding factor. g_{eff} is the effective air gap, it can be written as

$$g_{eff} = k_{cs} \cdot k_{cr}\ g \tag{4-13}$$

Where

k_{cs} the Carter factor for the stator slots

$$k_{cs} = \frac{\tau_s}{\tau_s - g\,\gamma_s} \tag{4-14}$$

$$\gamma_s = \frac{4}{\pi}\left(\frac{b_{s0}}{2g}\arctan\left(\frac{b_{s0}}{2g}\right) - \ln\sqrt{1+\left(\frac{b_{s0}}{2g}\right)^2}\right) \tag{4-15}$$

k_{cr} the Carter factor for the rotor slots

$$k_{cr} = \frac{\tau_r}{\tau_r - g\,\gamma_r} \tag{4-16}$$

$$\gamma_r = \frac{4}{\pi}\left(\frac{b_{r0}}{2g}\arctan\left(\frac{b_{r0}}{2g}\right) - \ln\sqrt{1+\left(\frac{b_{r0}}{2g}\right)^2}\right) \tag{4-17}$$

Where b_{r0} is the width of the rotor slot opening.

3. Rotor resistance and inductance

The rotor bar resistance is calculated as

$$R_{rb} = \frac{\rho_{cu} k_m\ L_t}{A_{cur} Q_r} \tag{4-18}$$

Where Q_r is the number of the rotor slots; k_m is the equivalent winding coefficient; A_{cur} is the cross-sectional area of the rotor conductor, which can be given as

$$A_{cur} = \frac{N_p\ q\, b_r (h_r - h_w)}{N_r} \tag{4-19}$$

Where N_r is the number of turns of the rotor; b_r and h_r are the width and height of the rotor slot, respectively.

The rotor end ring resistance is calculated as

$$R_{re} = \frac{\rho_{cu}\ k_m\ D_r}{2\pi\ N_p\ S_r} \tag{4-20}$$

Where D_r, S_r are the mean diameter and cross-sectional area of an end ring, respectively.

The phase resistance of the rotor is the sum of the rotor bar resistance and the rotor end ring resistance.

$$R_r = R_{rb} + R_{re} \tag{4-21}$$

The rotor leakage inductance, tooth tip leakage inductance and end winding leakage inductance can be also expressed as

$$L_{rsl} = 2\mu_0 \frac{L_t\ N_r^2}{N_p\ q}\left(\frac{(h_r - h_w)}{3b_r} + \frac{h_w}{b_{r0}}\right) \tag{4-22}$$

$$L_{rtl} = 2\mu_0 \frac{L_t\ N_r^2}{N_p\ q}\frac{5\ g / b_{r0}}{5 + 4\ g / b_{r0}} \tag{4-23}$$

$$L_{rel} = \mu_0 \frac{4\ N_r^2}{3\ N_p}\left(\frac{0.3\ D_r}{N_p} + 0.01\right) \tag{4-24}$$

The rotor leakage inductance $L_{r\sigma}$ can be given as the sum of the rotor slot, air-gap, and end-

winding leakage inductances.

$$L_{r\sigma} = L_{rsl} + L_{rtl} + L_{rel} \tag{4-25}$$

Fig. 4-2 illustrates the steady-state equivalent circuit of a SCIG.

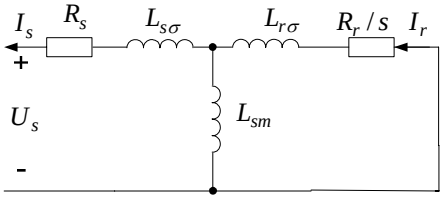

Fig. 4-2: *The steady-state equivalent circuit of a SCIG*

3. Power and losses

The no-load voltage induced by the air gap flux density in a stator winding can be calculated as

$$E_p = \sqrt{2}\, k_w \cdot N_s \cdot \omega_s \cdot r_s \cdot L_t \cdot B_{g1} \tag{4-26}$$

where ω_s is the synchronous angular speed of the magnetic field, B_{g1} is the fundamental space harmonic of the air gap flux density.

The air gap power can be calculated according to the mechanical power and the slip.

$$P_e = P_{mec} /(1-s) \tag{4-27}$$

The rotor active current can be expressed as

$$I_r = \sqrt{sP_e / m / R_r} \tag{4-28}$$

The stator reactive current can be also expressed as

$$I_{sm} = E_p /(2\pi\ f\ L_{sm}) \tag{4-29}$$

Therefore, the stator phase current

$$I_s = \sqrt{(I_r^2 + I_{sm}^2)} \tag{4-30}$$

The stator and rotor cooper losses are written as :

$$p_{cus} = m\, I_s^2 R_s \tag{4-31}$$

$$p_{cur} = m\, I_r^2 R_r \tag{4-32}$$

The specific iron losses (the iron losses per unit mass) are approximated with Steinmetz formula by using [9] [36]

$$p_{Fe} = 2\, p_{Fe0h} \cdot (\frac{f_e}{f_0})(\frac{\widehat{B}_{Fe}}{\widehat{B}_0})^2 + 2\, p_{Fe0e} \cdot (\frac{f_e}{f_0})^2 (\frac{\widehat{B}_{Fe}}{\widehat{B}_0})^2 \tag{4-33}$$

where f_e is the frequency of the field in the iron, p_{Fe0h} and p_{Fe0e} are the specific hysteresis loss and the specific eddy current loss (in W/kg) in the laminated stator core, for a given frequency f_0 (50Hz) and a flux density $\widehat{B}_0$ (1.5T)

To calculate the total iron losses, the specific iron losses in the different parts (teeth and yokes) are evaluated, multiplied by the weight of these parts, and added.

4. Mass and cost of active material

The total mass and cost of active material are given by

$$m_{act} = m_{cus} + m_{cur} + m_{Fest} + m_{Fesy} + m_{Fert} + m_{Fery} \tag{4-34}$$

$$C_{act} = c_{cu}(m_{cus} + m_{cur}) + c_{Fe}(m_{Fest} + m_{Fesy} + m_{Fert} + m_{Fery}) \tag{4-35}$$

Where

m_{cus} is the mass of the stator copper, $m_{cus} = \rho_{cu}(m\, L_{cus}\, A_{cus})$;

m_{cur} is the mass of the rotor copper, $m_{cur} = \rho_{cu}(Q_r\, L_t\, A_r + 2\pi D_r S_r)$;

m_{Fest} is the iron mass of the stator tooth, $m_{Fest} = \rho_{Fe}(\pi L_t\, ((r_s + h_s)^2 - r_s^{\,2}) - 2m\, q\, N_p\, b_s\, h_s\, L_t)$;

m_{Fesy} is the iron mass of the stator yoke, $m_{Fesy} = \rho_{Fe}(\pi L_t\, ((r_s + h_s + h_{sy})^2 - (r_s + h_s)^2)$;

m_{Fert} is the iron mass of the rotor tooth, $m_{Fert} = \rho_{Fe}(\pi L_t\, (r_r^{\,2} - (r_r - h_r)^2) - 2m\, q\, N_p\, b_r\, h_r\, L_t)$;

m_{Fery} is the iron mass of the rotor yoke, $m_{Fery} = \rho_{Fe}(\pi L_t\, ((r_r - h_r)^2 - (r_r - h_r - h_{ry})^2)$;

c_{cu} c_{Fe} are the specific cost of the copper and the iron, respectively.

4.2 Model description of DFIG

The stator slot of a DFIG is chosen as the same as that of the SCIG, which is shown in Fig. 4-1, so the calculations of stator slot dimensions, the stator resistance and inductance, mass of the active materials are similar, which are presented in the subsection 4.1. In the following, the rotor resistance and inductance, power calculations and mass weight are described, respectively.

1. Rotor resistance and inductance

The rotor slot is also semi-closed, and the rotor winding resistance can be calculated as

$$R_r = \frac{\rho_{cu} L_{cur}}{A_{cur}} \tag{4-36}$$

where ρ_{cu} is the resistivity of copper. A_{cur} is the cross-sectional area of the rotor conductor, and L_{cur} is the length of the conductor of the rotor phase winding, which can be given as

$$L_{cur} = 2\, N_r (2(\tau_p - \tau_s) + L_t) \tag{4-37}$$

$$A_{cur} = k_{fillr} \frac{N_p\, q\, b_r (h_r - h_w)}{N_r} \tag{4-38}$$

Where k_{fillr} is the rotor slot fill factor; L_t is the core length (in this case, the rotor core length is assumed as the same as the stator core length);

The rotor leakage inductance, tooth tip leakage inductance and end winding leakage inductance can be expressed as

$$L_{rsl} = 2\,\mu_0 \frac{L_t\, N_r^2}{N_p\, q} \left(\frac{(h_r - h_w)}{3 b_r} + \frac{h_w}{b_{r0}}\right) \tag{4-39}$$

$$L_{rtl} = 2\,\mu_0 \frac{L_t\, N_r^2}{N_p\, q} \frac{5\, g / b_{r0}}{5 + 4\, g / b_{r0}} \tag{4-40}$$

$$L_{rel} = \mu_0 \frac{1.2\, N_r^2}{N_p} \left(\frac{2}{3}\tau_p + 0.01\right) \tag{4-41}$$

The rotor inductance, L_r can be given as the sum of the magnetizing inductance, slot, air-gap, and end-winding leakage inductances.

$$L_r = L_{sm} + L_{rsl} + L_{rtl} + L_{rel} \tag{4-42}$$

To simplify the calculations, the equivalent circuit of the DFIG is used as shown in Fig. 4-3. The parameters can be calculated as [9]:

$$\sigma = 1 - \frac{L_{sm}^2}{L_s \; L_r} \tag{4-43}$$

$$L_s = L_{sm} + L_{ssl} + L_{stl} + L_{sel} \tag{4-44}$$

$$R_R = R_r \frac{L_s^2}{L_{sm}^2} \tag{4-45}$$

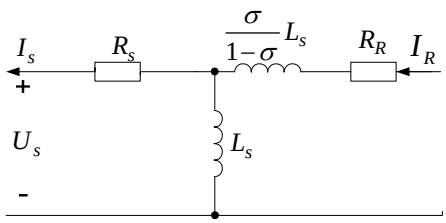

Fig. 4-2: *The steady-state equivalent circuit of a DFIG*

2. Power and losses

The no-load voltage induced by the air gap flux density in a stator winding can be calculated as

$$E_p = \sqrt{2}\, k_w \cdot N_s \cdot \omega_s \cdot r_s \cdot L_t \cdot B_{g1} \tag{4-46}$$

The air gap power can be calculated according to the mechanical power and the slip.

$$P_e = P_{mec} /(1-s) \tag{4-47}$$

The rotor active current (in this case, the rotor power facto is assumed to be 1) can be expressed as

$$I_R = P_e / m / E_p \tag{4-48}$$

The stator reactive current can be also expressed as

$$I_{sm} = E_p /(2\pi \; f \; L_s) \tag{4-49}$$

Therefore, the stator phase current

$$I_s = \sqrt{(I_R^2 + I_{sm}^2)} \tag{4-50}$$

The stator and rotor cooper losses are written as :

$$p_{cus} = m \, I_s^2 R_s \tag{4-51}$$

$$p_{cur} = m \, I_R^2 R_R \tag{4-52}$$

3. Mass and cost of active material

The total mass and cost of active material are given by

$$m_{act} = m_{cus} + m_{cur} + m_{Fest} + m_{Fesy} + m_{Fert} + m_{Fery} \tag{4-53}$$

$$C_{act} = c_{cu}(m_{cus} + m_{cur}) + c_{Fe}(m_{Fest} + m_{Fesy} + m_{Fert} + m_{Fery}) \tag{4-54}$$

Where

m_{cus} is the mass of the stator copper, $m_{cus} = \rho_{cu}(m\ L_{cus}\ A_{cus})$;

m_{cur} is the mass of the rotor copper, $m_{cus} = \rho_{cu}(m\ L_{cur}\ A_{cur})$;

m_{Fest} is the iron mass of the stator tooth, $m_{Fest} = \rho_{Fe}(\pi\ L_t\ ((r_s + h_s)^2 - r_s{}^2) - 2m\,q\ N_p\ b_s\ h_s\ L_t)$;

m_{Fesy} is the iron mass of the stator yoke, $m_{Fesy} = \rho_{Fe}(\pi\ L_t\ ((r_s + h_s + h_{sy})^2 - (r_s + h_s)^2)$;

m_{Fert} is the iron mass of the rotor tooth, $m_{Fert} = \rho_{Fe}(\pi\ L_t\ (r_r{}^2 - (r_r - h_r)^2) - 2m\,q\ N_p\ b_r\ h_r\ L_t)$;

m_{Fery} is the iron mass of the rotor yoke, $m_{Fery} = \rho_{Fe}(\pi\ L_t\ ((r_r - h_r)^2 - (r_r - h_r - h_{ry})^2)$;

c_{cu} c_{Fe} are the specific cost of the copper and the iron, respectively.

5. Design models of synchronous generators

The synchronous generator parameters are also calculated based on well-known analytical methods using equivalent circuit models. The dimensions of the active parts can be obtained from the conventional magnetic circuit laws. This section is to describe the key analytical models used to determine the synchronous generator sizes and the important equations used to determine the parameters of the equivalent circuit. More detailed about the calculations are given in [9] [16] [17] [36]. In addition, the corresponding optimization models and the design assumptions will be presented in report 2. The section 5 outline is as follows:

5.1 Model description of EESG: This subsection introduces the design equations of salient pole EESG, such as the machines basic dimensions, magnetic circuit, electrical parameters and power losses and so on.

5.2 Model description of PMSG: This subsection introduces the design equations of radial-flux PMSG, such as the machines basic dimensions, magnetic circuit, electrical parameters and power losses and so on.

5.1 Model description of EESG

In a direct-drive EESG design, the number of slots per pole and phase q is set to 2. Increasing this number makes the machine heavier and more expensive because of the increasing dimensions of end-windings and yokes. Decreasing this number results in a significant increase of the excitation losses, mainly in part load. Fig. 5-1 depicts a cross-section of half pole of the EESG.

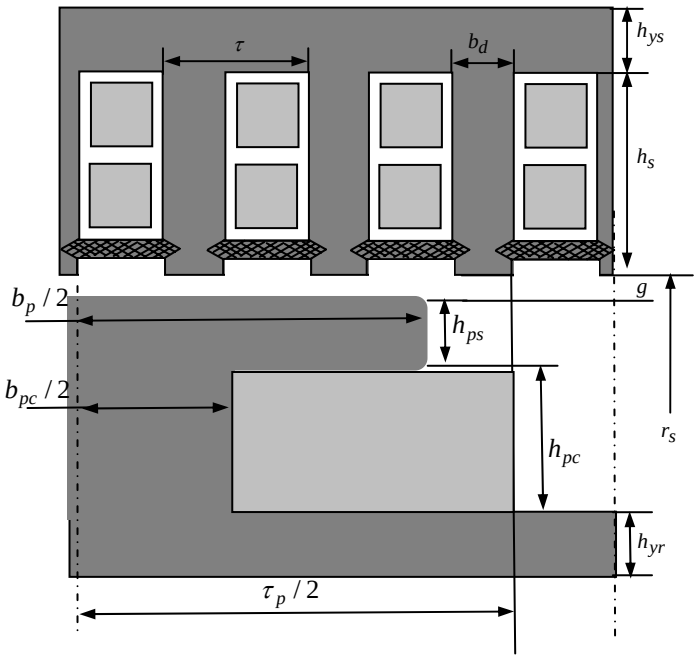

Fig. 5-1: *The construction of stator slots and rotor poles of an EESG*

1. Basic dimensions

The air gap diameter, d and pole pitch, τ_p can determine the number of pole pairs, N_p

$$N_p = \frac{\pi \cdot d}{2 \cdot \tau_p} \tag{5-1}$$

The air gap is calculated as

$$g = 0.001\, d \tag{5-2}$$

However, the minimum air gap is limited to be 5mm due to the mechanical stiffness and the thermal expansion.

The output frequency at the rated speed is

$$f = \frac{n_r \cdot Np}{60} \tag{5-3}$$

Where n_r is the generator rotor speed.

The stator slot pitch is

$$\tau_s = \frac{\tau_p}{m \cdot q} \tag{5-4}$$

The stator yoke thickness h_{ys}, is determined by the allowed flux densities in the stator yokes.

$$h_{ys} = \frac{\hat{B}_{g0} \cdot \tau_p}{\hat{B}_{ys} \cdot \pi} \tag{5-5}$$

Where $\hat{B}_{g0}$ is the peak air gap flux density; $\hat{B}_{ys}$ is the peak stator and rotor yoke flux density. In this case, the rotor yoke thickness *hyr* is assumed to be the same of the stator yoke thickness.

The pole shoe width b_p is kept at 0.7 times the pole pitch:

$$b_p = 0.7\, \tau_p \tag{5-6}$$

The rotor pole shoe height at center h_{ps} should be large enough to accommodate the damper winding and is proportional to the pole pitch [36]:

$$h_{ps} = 0.1\, \tau_p \tag{5-7}$$

The pole body width b_{pc} and height h_{pc} are chosen as [36]:

$$b_{pc} = 0.4\, \tau_p \tag{5-8}$$

$$h_{pc} = 0.6\, \tau_p \tag{5-9}$$

2. Stator resistance and inductance

The phase resistance is calculated as

$$R_s = \frac{\rho_{cu} L_{cus}}{A_{cus}} \tag{5-10}$$

where ρ_{cu} is the resistivity of copper. A_{cus} is the cross-sectional area of the stator conductor, and L_{cus} is the length of the conductor of the stator phase winding, which can be given as

$$L_{cus} = 2\, N_s (2\,(\tau_p - shortpitch / m / q) + L_t) \tag{5-11}$$

$$A_{cus} = k_{fills} \frac{N_p\, q\, b_s (h_s - h_w)}{N_s} \tag{5-12}$$

Where *shortpitch* is numbers of the stator winding short-pitched; k_{fills} is the stator slot fill factor; L_t is the stator core length; h_w is the slot wedge thickness, N_s is the number of turns of the stator

The stator slot leakage inductance, tooth tip leakage inductance and end winding leakage inductance can be expressed as

$$L_{ssl} = 2\,\mu_0 \frac{L_t\ N_s^2}{N_p\ q}\left(\frac{(h_s - h_w)}{3b_s} + \frac{h_w}{b_{s0}}\right) \tag{5-13}$$

$$L_{stl} = 2\,\mu_0 \frac{L_t\ N_s^2}{N_p\ q}\frac{5\ g / b_{s0}}{5 + 4\ g / b_{s0}} \tag{5-14}$$

$$L_{sel} = \mu_0 \frac{1.2\ N_s^2}{N_p}\left(\frac{2}{3}\tau_p + 0.01\right) \tag{5-15}$$

Where μ_0 is the constant of the permeability of vacuum; b_s is the stator slot width; b_{s0} is the width of the stator slot opening.

The stator leakage inductance $L_{s\sigma}$ can be given as the sum of the slot, air-gap, and end-winding leakage inductances.

$$L_{s\sigma} = L_{ssl} + L_{stl} + L_{sel} \tag{5-16}$$

The magnetizing inductance is given as [9] [36]

$$L_m = \frac{6 \cdot \mu_0 \cdot L_t \cdot r_s \cdot (k_w \cdot N_s)^2}{\pi \cdot Np^2 g_{eff}} \tag{5-17}$$

where r_s is the stator radius, k_w is the stator winding factor. g_{eff} is the effective air gap.

The *d* and *q* magnetizing inductances:

$$L_{dm} = K_d\ L_m = \left(\frac{b_p}{\tau_p} + \frac{1}{\pi}\sin(\pi\frac{b_p}{\tau_p})\right) L_m \tag{5-18}$$

$$L_{qm} = K_q\ L_m = \left(\frac{b_p}{\tau_p} - \frac{1}{\pi}\sin(\pi\frac{b_p}{\tau_p}) + \frac{2}{3\pi}\cos(\frac{b_p}{\tau_p}\frac{\pi}{2})\right) L_m \tag{5-19}$$

The synchronous magnetizing inductances:

$$L_d = L_{dm} + L_{s\sigma} \tag{5-20}$$

$$L_q = L_{qm} + L_{s\sigma} \tag{5-21}$$

Fig. 5-2 and Fig. 5-3 depict the equivalent circuit of the EESG and the applied phasor diagram, respectively.

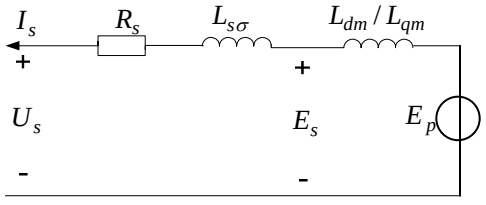

Fig. 5-2: *The steady-state equivalent circuit of an EESG*

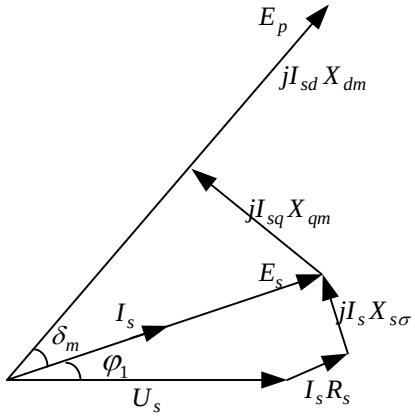

Fig. 5-3: *The applied phasor diagram of an EESG*

In Fig. 5-3, the phase current leads the phase voltage a little in order to reduce saturation and excitation losses while a larger rating of the converter is not necessary [17][23].

3. Excitation resistance and leakage inductance

The field-winding resistance is calculated as

$$R_r = \frac{\rho_{cu} L_{cur}}{A_{cur}} \tag{5-22}$$

Where

$$L_{cur} = 4\, N_p\ N_f\ (L_t + b_{pc} + \frac{\pi}{4}(\frac{\pi(r_r - h_{pc} - h_{ps})}{N_p} - b_{pc})) \tag{5-23}$$

$$A_{cur} = k_{fillr}\ \frac{h_{pc}}{2\, N_f}(\frac{\pi(r_r - h_{pc} - h_{ps})}{N_p} - b_{pc}) \tag{5-24}$$

The main field inductance is calculated as

$$L_{fg} = 2\mu_0\ N_p\ L_t (2N_f)^2 (\frac{h_{ps}}{\tau_p - b_{ps}} + \frac{h_{pc}}{3(\frac{\pi(r_r - h_{pc} - h_{ps})}{N_p} - b_{pc})}) \tag{5-25}$$

Where r_r is the rotor outer radius, N_f is the number of turn for the excitation winding; k_{fillr} is the fill factor of the excited winding.

3. Power and losses

The no-load voltage induced by the air gap flux density in a stator winding can be calculated as [11]

$$E_s = \sqrt{2}\ k_w \cdot N_s \cdot \omega_m \cdot r_s \cdot L_t \cdot B_{g1} \tag{5-26}$$

where ω_m is the mechanical angular speed of the rotor, B_{g1} is the fundamental space harmonic of the air gap flux density.

According to the applied phasor diagram shown in Fig. 5-3, the following equation can be obtained

$$E_s = I_s R_s + U_s \cos\varphi_1 = I_s R_s + \frac{P_g}{m I_s} \tag{5-27}$$

Where $\cos\varphi_1$ is the stator power factor; P_g is the output power of the generator.

Thus the stator current can be calculated by solving the above equation:

$$I_s = \frac{E_s - \sqrt{E_s^2 - 4\,R_s\,P_g\,/\,m}}{2\,R_s} \tag{5-28}$$

The excitation current can be also calculated by the phasor diagram [36].

$$I_f = \frac{E_p}{E_s} B_{g1} \cdot g_{eff} \cdot \frac{\pi}{4\,N_f\,\mu_0 \sin(\frac{\pi}{2}\frac{b_p}{\tau_p})} \tag{5-29}$$

where

$$\delta_m = \tan^{-1}(\omega_1\,L_{qm}\,I_s\,/\,E_s) \tag{5-30}$$

$$I_{sd} = I_s \sin(\delta_m) \tag{5-31}$$

$$I_{sq} = I_s \cos(\delta_m) \tag{5-32}$$

$$E_p = \omega_1 \cdot L_{dm} \cdot I_{sd} + \sqrt{E_s^2 - (\omega_1\,L_{qm}\,I_{sq})^2} \tag{5-33}$$

The stator and rotor cooper losses are written as:

$$p_{cus} = m\,I_s^2 R_s \tag{5-34}$$

$$p_{cur} = I_f^2 R_r \tag{5-35}$$

The specific iron losses (the iron losses per unit mass) are approximated with Steinmetz formula by using [4] [5]

$$p_{Fe} = 2\,p_{Fe0h} \cdot (\frac{f_e}{f_0})(\frac{\widehat{B}_{Fe}}{\widehat{B}_0})^2 + 2\,p_{Fe0e} \cdot (\frac{f_e}{f_0})^2 (\frac{\widehat{B}_{Fe}}{\widehat{B}_0})^2 \tag{5-36}$$

where f_e is the frequency of the field in the iron, p_{Fe0h} and p_{Fe0e} are the specific hysteresis loss and the specific eddy current loss (in W/kg) in the laminated stator core, for a given frequency f_0 (50Hz) and a flux density $\widehat{B}_0$ (1.5T)

To calculate the stator iron losses, the specific iron losses in the different parts (teeth and yokes) are evaluated, multiplied by the weight of these parts, and added.

4. Mass and cost of active material

The total mass and cost of active material are given by

$$m_{act} = m_{cus} + m_{cur} + m_{Fest} + m_{Fesy} + m_{Ferp} + m_{Fery} \tag{5-37}$$

$$C_{act} = c_{cu}(m_{cus} + m_{cur}) + c_{Fe}(m_{Fest} + m_{Fesy} + m_{Ferp} + m_{Fery}) \tag{5-38}$$

Where

m_{cus} is the mass of the stator copper, $m_{cus} = \rho_{cu}(m\,L_{cus}\,A_{cus})$;

m_{cur} is the mass of the rotor copper, $m_{cur} = \rho_{cu}(L_{cur}\,A_{cur})$;

m_{Fest} is the iron mass of the stator tooth, $m_{Fest} = \rho_{Fe}(\pi\,L_t\,((r_s + h_s)^2 - r_s^{\,2}) - 2m\,q\,N_p\,b_s\,h_s\,L_t)$;

m_{Fesy} is the iron mass of the stator yoke, $m_{Fesy} = \rho_{Fe}(\pi\,L_t\,((r_s + h_s + h_{sy})^2 - (r_s + h_s)^2)$;

m_{Fert} is the iron mass of the rotor pole, $m_{Fert} = \rho_{Fe}(2\,Np\,L_t(h_{pc}\,b_{pc} + b_{ps}\,h_{ps}))$;

m_{Fery} is the iron mass of the rotor yoke, $m_{Fery} = \rho_{Fe}(\pi\,L_t\,((r_r - h_{ps} - h_{pc})^2 - (r_r - h_{ps} - h_{pc} - h_{ry})^2)$;

c_{cu} c_{Fe} are the specific cost of the copper and the iron, respectively.

5.2 Model description of PMSG

A radial-flux PM (RFPM) machine with surface mounted magnets seems to be a better choice for low-speed, direct-drive large wind turbines due to its simple structure and reliability. In this case, a three-phase RFPM machine is chosen for comparison of the different wind turbine concepts with PM generator systems.

For a RFPM generator system, the number of slots per pole and phase, q is set to 1 to allow a small pole pitch without getting a low slot fill factor [17]. Compared with an EESG, decreasing this number does not result in a significant increase of the excitation losses, because permanent magnets are used. Fig. 5-4 illustrates one pole of a RFPM machine.

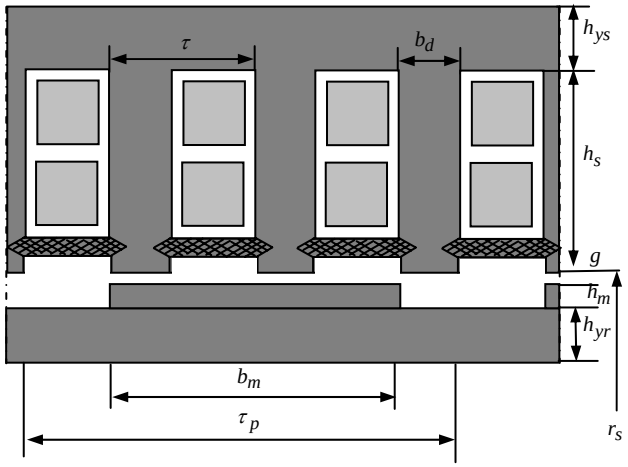

Fig. 5-4: *Basic dimension of one pole of a RFPM machine*

1. Basic dimensions

The air gap diameter, d and pole pitch, τ_p can determine the number of pole pairs, N_p

$$N_p = \frac{\pi \cdot d}{2 \cdot \tau_p} \tag{5-39}$$

The air gap is calculated as

$$g = 0.001\,d \tag{5-40}$$

However, the minimum air gap is limited to be 5mm for large direct-drive PMSG, due to the mechanical stiffness and the thermal expansion.

The output frequency at the rated speed is

$$f = \frac{n_r \cdot N_p}{60} \tag{5-41}$$

Where n_r is the generator rotor speed.

The stator slot pitch is

$$\tau_s = \frac{\tau_p}{m \cdot q} \tag{5-42}$$

The stator yoke thickness, h_{ys} is determined by the allowed flux densities in the stator yokes.

$$h_{ys} = \frac{\hat{B}_{g0} \cdot b_m \cdot L_e}{2 \cdot \hat{B}_{ys} \cdot L_u} \tag{5-43}$$

where b_m is the magnet width; $\hat{B}_{ys}$ is the peak stator yoke flux density; L_e is the equivalent core length; L_u is the available iron stack length. In this case, the stator and rotor yoke heights are assumed as the same value.

The magnet width b_m is kept at 70% of the pole pitch, but the minimum value is limited to be 3 times larger than the air gap thickness to reduce the tangential fringing flux of the PMs in the air gap [36].

$$b_m = 0.7\,\tau_p \tag{5-44}$$

The magnet thickness h_m as a function of air gap flux density is given [9] [16]

$$h_m = \frac{\hat{B}_{g0} \cdot \mu_{rm} \cdot g_{eff}}{B_{rm}} \tag{5-45}$$

where B_{rm} is the remanent flux density of the magnets (1.2T). μ_{rm} is the relative permeability of the permanent magnet material. g_{eff} is the effective air gap, which can be given as

$$g_{eff} = k_{cs} \cdot (g + \frac{h_m}{\mu_{rm}}) \tag{5-46}$$

where k_{cs} is the Carter factor for the stator slots [9].

$$k_{cs} = \frac{\tau_s}{\tau_s - (g + \frac{h_m}{u_{rm}})\gamma_s} \tag{5-47}$$

$$\frac{b_{s0}}{2(g + \frac{h_m}{\mu_{rm}})} \arctan(\frac{b_{s0}}{2(g + \frac{h_m}{\mu_{rm}})}) - \ln \sqrt{1 + (\frac{b_{s0}}{2(g + \frac{h_m}{\mu_{rm}})})^2} \tag{5-48}$$

2. Stator resistance and inductance

The phase resistance is calculated as

$$R_s = \frac{\rho_{cu} L_{cus}}{A_{cus}} \tag{5-49}$$

where ρ_{cu} is the resistivity of copper. A_{cus} is the cross-sectional area of the stator conductor, and L_{cus} is the length of the conductor of the stator phase winding, which can be given as

$$L_{cus} = 2\,N_s\,(2\,\tau_p + L_t) \tag{5-50}$$

$$A_{cus} = k_{fills}\,\frac{N_p\,q\,b_s\,(h_s - h_w)}{N_s} \tag{5-51}$$

Where k_{fills} is the stator slot fill factor; L_t is the stator core length; h_w is the slot wedge thickness, N_s is the number of turns of the stator phase winding.

The slot leakage inductance, tooth tip leakage inductance and end winding leakage inductance can be expressed as

$$L_{ssl} = 2\,\mu_0 \frac{L_t\ N_s^2}{N_p\ q}\left(\frac{(h_s - h_w)}{3b_s} + \frac{h_w}{b_{s0}}\right) \tag{5-52}$$

$$L_{stl} = 2\,\mu_0 \frac{L_t\ N_s^2}{N_p\ q}\frac{5\,g/b_{s0}}{5+4\,g/b_{s0}} \tag{5-53}$$

$$L_{sel} = \mu_0 \frac{1.2\ N_s^2}{N_p}\left(\frac{2}{3}\tau_p + 0.01\right) \tag{5-54}$$

The stator leakage inductance $L_{s\sigma}$ can be given as the sum of the slot, air-gap, and end-winding leakage inductances.

$$L_{s\sigma} = L_{ssl} + L_{stl} + L_{sel} \tag{5-55}$$

The magnetizing inductance is given as

$$L_{sm} = \frac{6 \cdot \mu_0 \cdot L_t \cdot r_s \cdot (k_w \cdot N_s)^2}{\pi \cdot Np^2 g_{eff}} \tag{5-56}$$

where r_s is the stator radius, k_w is the winding factor. g_{eff} is the effective air gap.

The synchronous magnetizing inductances:

$$L_s = L_{sm} + L_{s\sigma} \tag{5-57}$$

Fig. 5-5 and Fig. 5-6 depict the equivalent circuit of the EESG and the applied phasor diagram, respectively.

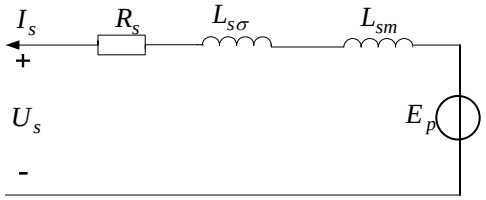

Fig. 5-5: *The steady-state equivalent circuit of a PMSG*

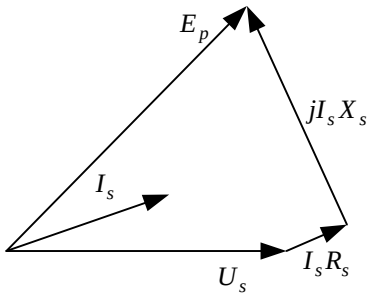

Fig. 5-6: *The applied phasor diagram of a PMSG*

In Fig. 5-6, the armature phase current is in the middle between the terminal voltage U_s and the internal electromotive force (emf) E_p, induced by the magnets, in order to introduce the lowest power rating requirements on both generator and rectifier, and to utilize the PMSG and converter best.

2. Power and losses

The fundamental harmonic of the air gap flux density can be calculated as

$$B_{g1} = B_{rm} \frac{h_m}{\mu_{rm}\, g_{eff}} \cdot \frac{4}{\pi}\sin\left(\frac{\pi \cdot b_m}{2 \cdot \tau_p}\right) \tag{5-58}$$

The no-load voltage induced by this flux density in a stator winding can be calculated as [9]

$$E_P = \sqrt{2}\, k_w \cdot N_s \cdot \omega_m \cdot r_s \cdot L_t \cdot B_{g1} \tag{5-59}$$

where ω_m is the mechanical angular speed of the rotor, B_{g1} is the fundamental space harmonic of the air gap flux density.

The stator current can be calculated according to the applied phasor diagram.

$$I_s = \sqrt{\left(\frac{P_g}{m\, E_p}\right)^2 + \left(\frac{E_p - \sqrt{E_p^2 - (\omega_1 L_s)^2 \left(\frac{P_g}{m\, E_p}\right)^2}}{(\omega_1 L_s)^2}\right)^2} \tag{5-60}$$

Where P_g is the output power of the generator.

The stator cooper loss is written as

$$p_{cus} = m\, I_s^2 R_s \tag{5-61}$$

The specific iron losses (the iron losses per unit mass) are approximated with Steinmetz formula by using

$$p_{Fe} = 2\, p_{Fe0h} \cdot \left(\frac{f_e}{f_0}\right)\left(\frac{\hat{B}_{Fe}}{\hat{B}_0}\right)^2 + 2\, p_{Fe0e} \cdot \left(\frac{f_e}{f_0}\right)^2 \left(\frac{\hat{B}_{Fe}}{\hat{B}_0}\right)^2 \tag{5-62}$$

where f_e is the frequency of the field in the iron, p_{Fe0h} and p_{Fe0e} are the specific hysteresis loss and the specific eddy current loss (in W/kg) in the laminated stator core, for a given frequency f_0 (50Hz) and a flux density $\hat{B}_0$ (1.5T)

To calculate the stator iron losses, the specific iron losses in the different parts (teeth and yokes) are evaluated, multiplied by the weight of these parts, and added.

4. Mass and cost of active material

The total mass and cost of active material are given by

$$m_{act} = m_{cus} + m_{Fest} + m_{Fesy} + m_{Fery} + m_{PM} \tag{5-62}$$

$$C_{act} = c_{cu} m_{cus} + c_{Fe}(m_{Fest} + m_{Fesy} + m_{Fery}) + c_{PM}\, m_{PM} \tag{5-63}$$

Where

m_{cus} is the mass of the stator copper, $m_{cus} = \rho_{cu}(m\, L_{cus}\, A_{cus})$;

m_{Fest} is the iron mass of the stator tooth, $m_{Fest} = \rho_{Fe}(2\, m\, N_p\, q\, L_t\ b_{st}\, h_s)$;

m_{Fesy} is the iron mass of the stator yoke, $m_{Fesy} = \rho_{Fe}(\pi\, L_t\, ((r_s + h_s + h_{sy})^2 - (r_s + h_s)^2)$;

m_{Fery} is the iron mass of the rotor yoke, $m_{Fery} = \rho_{Fe}(\pi\, L_t\, ((r_r - h_m)^2 - (r_r - h_m - h_{ry})^2)$;

m_{PM} is the mass of the PM, $m_{PM} = \rho_{PM}(4\, L_t\, r_r\, h_m \frac{b_m}{\tau_p})$;

c_{cu}, c_{Fe}, c_{PM} are the specific cost of the copper, the iron and the PM, respectively.

6. Conclusions

In this report, an overview of different topologies of wind generator systems has been presented. The basic configurations and characteristics of various wind generator systems based on contemporary wind turbine concepts have been described with their advantages and disadvantages. The promising direct-drive PM machines, such as RFPM, AFPM and TFPM machines, have been surveyed. The current market status and the developing trends of wind generator systems have been presented. It can be seen that the multiple-stage geared drive DFIG concept is still dominant on the current market. Additionally, the market shows interest in the direct-drive or geared-drive concepts with a full-scale power electronic converter. Current developments of wind turbine concepts are mostly related to offshore wind energy, variable speed concepts with power electronics will continue to dominate and be very promising technologies for large wind farms. Moreover, the performance of PM materials is improving and the cost of PM materials is decreasing in recent years, which make variable speed direct-drive PM machines with a full-scale power converter more attractive for offshore wind power generations. With the increasing levels of wind turbine penetration in modern power systems, grid connection issues have posed several new challenges to wind turbine design and development. The future success of different wind turbine concepts will strongly depend on their ability of complying with both market expectations and the requirements of grid utility companies.

By the investigations of the current wind turbines concepts, the four types of generators, such as SCIG, DFIG, EESG and PMSG, are studied in this report, and seven variable speed wind turbine concepts, SCIG_3G, DFIG_3G, DFIG_1G, EESG_DD, PMSG_DD, PMSG_1G and PMSG_3G are further investigated to identify the most cost-effective choice.

As for the basic analytical models of design optimization of various wind generator systems, the design models of wind generator systems have been described in this report, including the wind turbine power characteristics, the models of the single-stage planetary gearbox and the three-stage gearbox, the models of the power electronic converter, and the electromagnetic design models of SCIG, DFIG, EESG and PMSG. The presented models may be useful for the preliminary designs of various wind generator systems. The demonstrations of the analytical models and the design optimization will be introduced in report 2.

References

[1] Z. Chen, F. Blaabjerg, “WIND ENERGY-The World's Fastest Growing Energy Source”, IEEE Power Electronics Society Newsletter, Volume18, Number 3, 2006, ISSN 1054-7231.

[2] Global Wind Energy Council (GWEC), “Global Wind 2006 Report”: http://www.gwec.net/uploads/media/gwec-2006_final.pdf

[3] A. D. Hansen, L. H. Hansen, “Wind turbine concept market penetration over 10 years (1995-2004)”, Wind Energy, (in press), DOI:10.1002/we.210.

[4] I. Erlich, W. Winter, A. Dittrich, “Advanced grid requirements for the integration of wind turbines into the German transmission system”, IEEE Power Engineering Society General Meeting, 18-22 June 2006.

[5] Z. Chen, F. Blaabjerg, “Wind Turbines-A Cost Effective Power Source”, Przeglad Elektrotechniczny R. 80 NR 5/2004 pp 464-469 (ISSN 0033-2097).

[6] F. Blaabjerg, Z. Chen, S. B. Kjaer, “Power Electronics as Efficient Interface in Dispersed Power Generation Systems”, IEEE Trans. on Power Electronics, Vol. 19, No. 5, Sept. 2004, pp. 1184-1194.

[7] R. Harrison, E. Hau and H. Snel, “Large wind turbines Design and Economics,” John Wiley & Sons Ltd, 2000, ISBN 0471-494569.

[8] S. Siegfriedsen and G. Bohmeke, “Multibrid Technology-A significant step to multi-megawatt wind turbines,” in Wind Energy, vol. 1, 1998, pp. 89-100.

[9] H. Polinder, F.F.A. van der Pijl, G.J. de Vilder, P. Tavner, “Comparison of direct-drive and geared generator concepts for wind turbines”, IEEE Trans. Energy Conversion, Vol. 21, pp. 725-733, September 2006.

[10] L. H. Hansen, L. Helle, F. Blaabjerg, E. Ritchie, etc, “Conceptual survey of generators and power electronics for wind turbines”, Riso national laboratory, Technical Report Riso-R-1205(EN), Roskilde, Denmark, December 2001..

[11] H. Polinder and J. Morren, “Developments in wind turbine generator systems”, Electrimacs 2005, Hammamet, Tunisia.

[12] M. R. Dubois, H. Polinder, and J. A. Ferreira, “Comparison of generator topologies for direct-drive wind turbines”, Proceedings of the Nordic Countries Power and Industrial Electronics Conference (NORPIE), Aalborg, Denmark , June 2000, pp. 22-26.

[13] O. Carlson, A. Grauers, J. Svensson, A. Larsson, “A comparison of electrical systems for variable speed operation of wind turbines”, European wind energy conf., pp.500-505, 1994.

[14] G. Bywaters, V. John, J. Lynch, P. Mattila, G. Nortor, J. Stowell, M. Salata, O. Labath, A. Chertok and D. Hablanian, “Northern power systems windPACT drive train alternative design study report”, NREL, Golden, Colorado, report No. NREL/SR-500-35524, October 2004.

[15] J. Soens,“Impact of wind energy in a future”, Ph. D dissertation, ISBN 90-5682-652-2, Wettelijk depot,UDC 621.548, Dec., 2005.

[16] M. R. Dubois, “Optimized permanent magnet generator topologies for direct-drive wind turbines”, Ph.D. dissertation, Delft Univ. Technol., Delft, The Netherlands, 2004.

[17] A. Grauers; “Design of direct-driven permanent-magnet generators for wind turbines”, PhD dissertation, Chalmers University of Technology, Goteburg, 1996.

[18] C. J. A. Versteegh, G. Hassan, “Design of the Zephyros Z72 wind turbine with emphasis on the direct drive PM generator”, NORPIE 2004, NTNU Trondheim Norway, 14-16 June, 2004.

[19] Y. Chen, P. Pillay, A. Khan, “PM wind generator topologies”, in IEEE Trans. on Industry Applications, Vol.41, No.6, Nov. 2005, pp.1619-1626.

[20] J. Chen, C. Nayar and L. Xu, “Design and finite-element analysis of an outer rotor permanent-magnet generator for directly-coupled wind turbine applications,” Proceedings of the IEEE Trans. on Magnetics, vol. 36, no. 5, September 2000, pp. 3802-3809.

[21] R. Hanitsch and G. Korouji, “Design and constructing of a permanent magnet wind energy generator with a new topology,” KOMEL Conf., Poland, May 2004, pp. 63-66.

[22] M. Aydin, S. Huang, T. A. Lipo, “Axial flux permanent magnet disc Machines: A review”, Research Report, 2004.

[23] M. R. Dubois, “Review of electromechanical conversion in wind turbines”, Report EPP00.R03, April, 2000.

[24] N. Bianchi, A. Lorenzoni, “Performance magnet generators for wind power industry: an overall comparison with traditional generators,” Opportunities and Advances in International Power generation, 18-20th March, 1996, pp. 49-54.
[25] M. S. Widyan, “Design, optimization, construction and test of rare-earth permanent-magnet electrical machines with new topology for wind energy applications”, Ph. D dissertation, Elektrotechnik und Informatik der Technischen Universität Berlin, July, 2006.
[26] A. Parviainen, “Design of axial-flux permanent-magnet low-speed machines and performance comparison between radial-flux and axial-flux machines”, Ph. D dissertation, Acta universitatis Lappeenrantaensis, 2005.
[27] P. Lampola, “Directly driven, low-speed permanent-magnet generators for wind power applications” PhD dissertation, Helsinki University of Technology, Finland, 2000.
[28] G. Böhmeke, R. Boldt, H. Beneke, “Geared Drive Intermediate Solutions-Comparisons of Design Features and Operating Economics,” in Proc. 1997 Europ. Wind Energy Conf., pp. 664-667.
[29] E. Spooner and A. C. Williamson, “Direct coupled, permanent magnet generators for wind turbine applications”, IEE Proc.-Electr. Power Appl., Vol. 143, No. 1, pp. 1-8, January 1996.
[30] E. Spooner and B. J. Chalmers, “TORUS : A slotless, toroidal-stator, permanent-magnet generator”, IEE Proceedings-B, Vol. 139, No. 6, pp. 497-506, November 1992.
[31] W. Wu, E. Spooner and B. J. Chalmers, “Design of slotless TORUS generators with reduced voltage regulation”, IEE Proc.-Electr. Power Appl., Vol. 142, No. 5, pp. 337-343, September 1995.
[32] W. Wu, E. Spooner and B. J. Chalmers, “Reducing voltage regulation in toroidal permanent-magnet generators by stator saturation”, in Proc. 1995 IEE Conf. Elec. Mach. And Drives, pp.385-389.
[33] Y. Chen, P. Pillay, “Axial-flux PM wind generator with a soft magnetic composite core”, in Proc. 2005 IEEE Conf. Ind. Appl., pp. 231-237.
[34] M. R. Harris, G. H. Pajooman and S. M. A. Sharkh, “Comparison of alternative topologies for VRPM(transverse-flux) electrical machines”, in Proc. 1997 IEE Colloquium on New Topologies for PM Machines, pp. 2/1-2/7.
[35] M. R. Harris, G. H. Pajooman and S. M. A. Sharkh, “The problem of power factor in VRPM (transverse-flux) machines”, in Proc. 1997 IEE Conf. Elec. Mach. and Drives, pp. 386-390.
[36] I. Boldea, “The electric generators handbook- Variable speed generators”, Taylor&Francis, 2006
[37] D. A. Torrey, “Switched Reluctance Generators and Their Control”, IEEE Transactions on Industrial Electronics, Vol.49, No. 1, February 2002, pp. 3-14.
[38] F. Runcos, R. Carlson, A. M. Oliveira, P. Kuo-Peng N. Sadowski, “Performance Analysis of a Brushless Double Fed Cage Induction Generator”, Nordic Wind Power Conference (NWPC04), Chalmers University of Technology, Göteborg, Sweden, March 1-2, 2004.
[39] ENERCON GmbH, http://www.enercon.de/en/_home.htm, last accessed November 2006.
[40] Winwind Oy, http://www.winwind.fi/english/tuotteet.html, last accessed September 2006.
[41] Harakosan Europe BV, http://www.harakosan.nl/products/, last accessed November 2006.
[42] Vestas Wind Systems, http://www.vestas.com/vestas/global/en/Downloads/Downloads/Download_brochurer.htm, last accessed September 2006.
[43] Siemens AG, http://www.powergeneration.siemens.com/en/windpower/products/index.cfm, last accessed September 2006.
[44] Repower Systems AG, http://www.repower.de/index.php?id=12&L=1, last accessed September 2006.
[45] Nordex AG, http://www.nordex-online.com/en/products-services/wind-turbines.html, last accessed September 2006.
[46] Multibrid , http://www.multibrid.com/m5000/data.html, last accessed September 2006.
[47] GE Energy, http://www.gepower.com/prod_serv/products/wind_turbines/en/index.htm, last accessed September 2006.
[48] Gamesa Elórica, http://www.gamesa.es/gamesa/index.html, last accessed September 2006.
[49] Ecotècnia, http://www.ecotecnia.com/index_ing.htm, last accessed September 2006.
[50] DeWind, http://www.dewind.de, last accessed September 2006.

[51] Suzlon Energy, http://www.suzlon.com/product_overview.htm, last accessed September 2006.
[52] BTM Consults. “International Wind Energy Department—World Market Update 2004, Forecast 2005–2009”. A. Rasmussens, Ringkøbing, Denmark, 2005.
[53] Z. Chen, “Issues of Connecting Wind Farms into Power Systems”, Proc. of 2005 IEEE/PES Transmission and Distribution Conference & Exhibition: Asia and Pacific. (Invited paper panel presentation paper).
[54] P. Sørensen, B. Bak-Jensen, J. Kristian, A. D. Hansen, L. Janosi, J. Bech, “Power plant characteristics of wind farms”, Wind Power for the 21st Century Proceedings of International Conference, Kassel, 2000; 176–179.
[55] H. Polinder, S.W.H. de Haan, M.R. Dubois, J.G. Slootweg, ‘Basic operation principles and electrical conversion systems of wind turbines'. In EPE Journal, December 2005 (vol. 15, no. 4), pp. 43-50.
[56] S. H. Jangamshetti, Dr. V. Guruprasada Rau, “Site matching of wind turbine generators: A case study”, IEEE Trans. on Energy Conversion, Vol. 14, no. 4, Dec. 1999, pp. 1537-1543.
[57] A. H. Marafia, and A. Ashour, “Economics of off-shore/on-shore wind energy systems in Qatar”, Renewable Energy, 28, 2003, pp. 1953-1963.
[58] R. Poore and T. Lettenmaier, “Alternative design study report: WindPACT advanced wind turbine drive train designs study”, NREL, Golden, Colorado, report No. NREL/SR-500-33196, August 2003.
[59] L. Fingersh, M. Hand, and A. Laxson, “Wind turbine design cost and scaling model”, Technical report NREL/TP-500-40566, Dec., 2006.